MSE

Carnegie Mellon

Grain Boundary Properties: **Energy**

27-750

Texture, Microstructure & Anisotropy

A.D. Rollett

With thanks to:
G.S. Rohrer, D. Saylor,
C.S. Kim, K. Barmak, W. Frazier, others …

Updated 3rd April, 2016

References

- Interfaces in Crystalline Materials, Sutton & Balluffi, Oxford U.P., 1998. Very complete compendium on interfaces.
- Interfaces in Materials, J. Howe, Wiley, 1999. Useful general text at the upper undergraduate/graduate level.
- Grain Boundary Migration in Metals, G. Gottstein and L. Shvindlerman, CRC Press, 1999. The most complete review on grain boundary migration and mobility. 2nd edition: ISBN: 9781420054354.
- Materials Interfaces: Atomic-Level Structure & Properties, D. Wolf & S. Yip, Chapman & Hall, 1992.
- See also publication lists by G.S. Rohrer and others for papers on grain boundary characterization and energy by researchers connected with the Mesoscale Interface Mapping Project ("MIMP").

Outline

- Motivation, examples of anisotropic grain boundary properties
- Grain boundary energy
  - Overview of GB energy
  - Low angle boundaries
  - Measurement methods
  - Herring relations, Young's Law
  - Extraction of GB energy from dihedral angles
  - Surface Grooves
  - High angle boundaries
  - Boundary plane vs. CSL
  - Simulation of grain growth
  - Capillarity Vector

1 / 2 / 3 / 5 -parameter GB Character Distribution

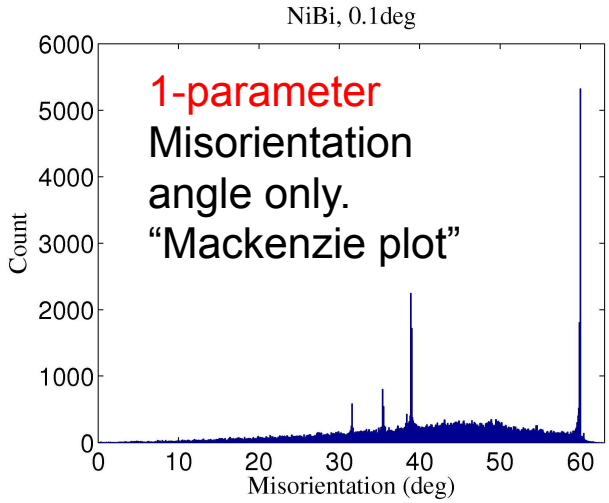

http://mimp.materials.cmu.edu

5-parameter
Grain Boundary Character Distribution – "GBCD".
Each misorientation type expands to a stereogram that shows variation in frequency of GB normals.

2-parameter
Grain Boundary Plane Distribution – "GBPD".
Shows variation in frequency of *GB normals only*, averaged over misorientation.

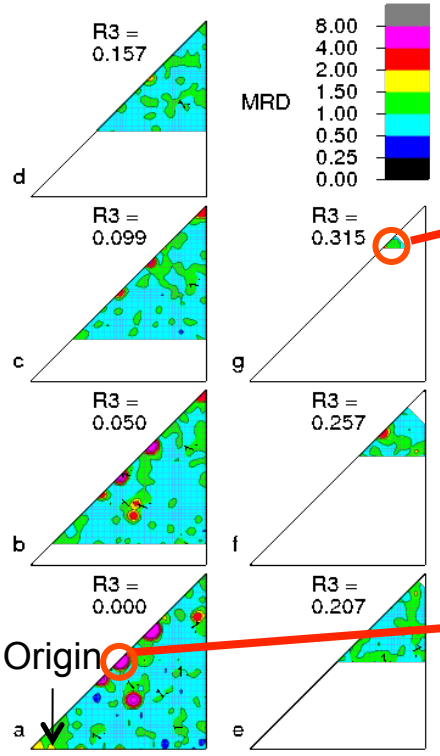

3-parameter
Misorientation Distribution
"MDF"
Rodrigues-Frank space

1.0 1.0 1.0 60.0

Σ3

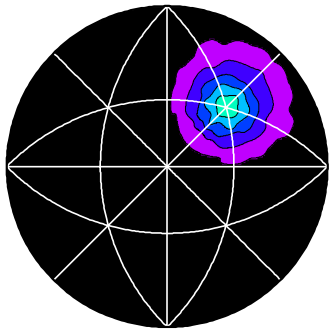

1.0 1.0 0.0 38.9

Σ9

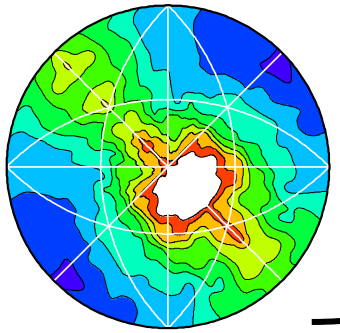

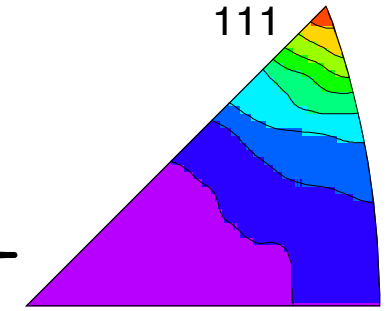

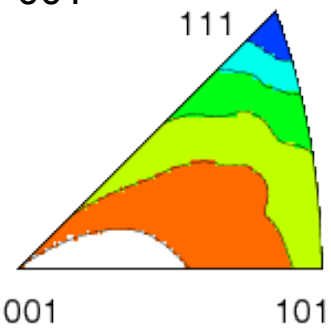

Ni surface energy [Foiles]

Example: Bi-doped Ni

Why learn about grain boundary properties?

- Many aspects of materials processing, properties and performance are affected by grain boundary properties.
- Examples include:
  - stress corrosion cracking in Pb battery electrodes, Ni-alloy nuclear fuel containment, steam generator tubes, aerospace aluminum alloys
  - creep strength in high service temperature alloys
  - weld cracking (under investigation)
  - electromigration resistance (interconnects)
- Grain growth and recrystallization, e.g. grain size control in ceramics
- Precipitation of second phases at grain boundaries depends on interface energy (& structure).

Properties, phenomena of interest

1. Energy (interfacial excess free energy → grain growth, coarsening, wetting, precipitation)
2. Mobility (normal motion in response to differences in stored energy → grain growth, recrystallization)
3. Sliding (tangential motion → creep)
4. Cracking resistance (intergranular fracture)
5. Segregation of impurities (embrittlement, formation of second phases), especially where they lead to *complexion transitions*.

Grain Boundary Diffusion

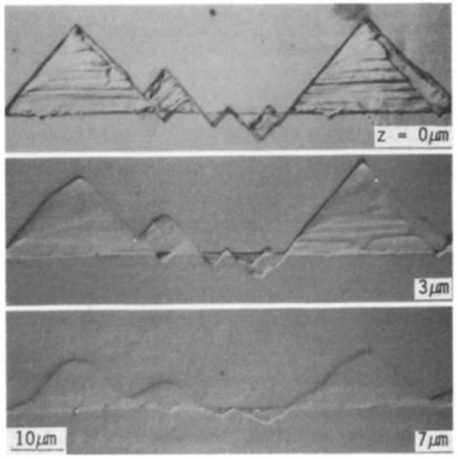

Fig. 6. DIGM of a symmetric Σ19a{133} tilt boundary exhibiting facets. Note that the sharp facets round off with increasing depth z beneath the surface. 14 h at 693 K; LM.

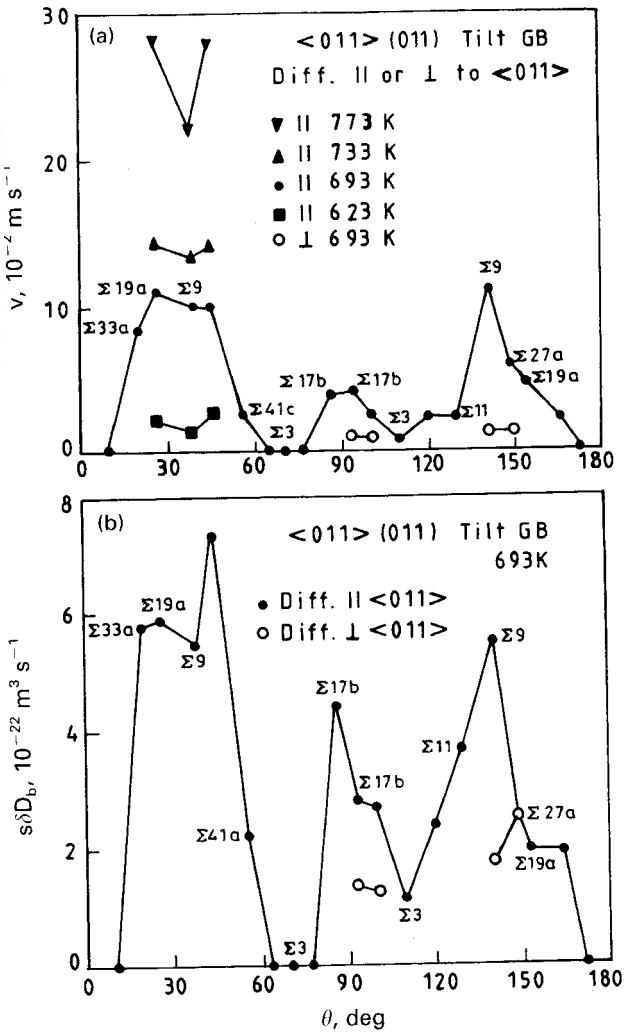

38 Kinetics of diffusion induced grain boundary migration in Cu bicrystals exposed to Zn vapour in terms of *a* variation of boundary velocity *v*, and *b* grain boundary chemical diffusion triple product $s\delta D_b$, as function of boundary misorientation angle θ for diffusion parallel (∥) and perpendicular (⊥) to ⟨011⟩ tilt axis of symmetric grain boundaries (GBs) with specific Σ values (*see* Ref. 100)

- Especially for high symmetry boundaries, there is a very strong anisotropy of diffusion coefficients as a function of boundary type. This example is for Zn diffusing into a series of <110> symmetric tilt boundaries in copper. Since this was an experiment on *diffusion induced grain boundary migration* (DIGM), see the figure above, the upper graph shows the migration velocity. The lower graph shows grain boundary diffusion coefficients.
- Note the low diffusion rates along low energy boundaries, especially Σ3.

Schmelze et al., *Acta mater.* **40** 997 (1992)

Grain Boundary Sliding

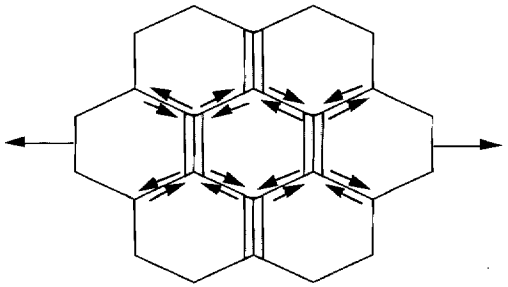

Figure 7.9 An array of grains showing the coupling between grain boundary sliding and diffusional elongation. (Adapted from Cook and Pharr, 1994, reproduced courtesy of VCH Publishers, Weinheim, Germany.)

- Grain boundary sliding should be very structure dependent. Reasonable therefore that Biscondi's results show that the rate at which boundaries slide is highly dependent on misorientation; in fact there is a threshold effect with no sliding below a certain misorientation at a given temperature.

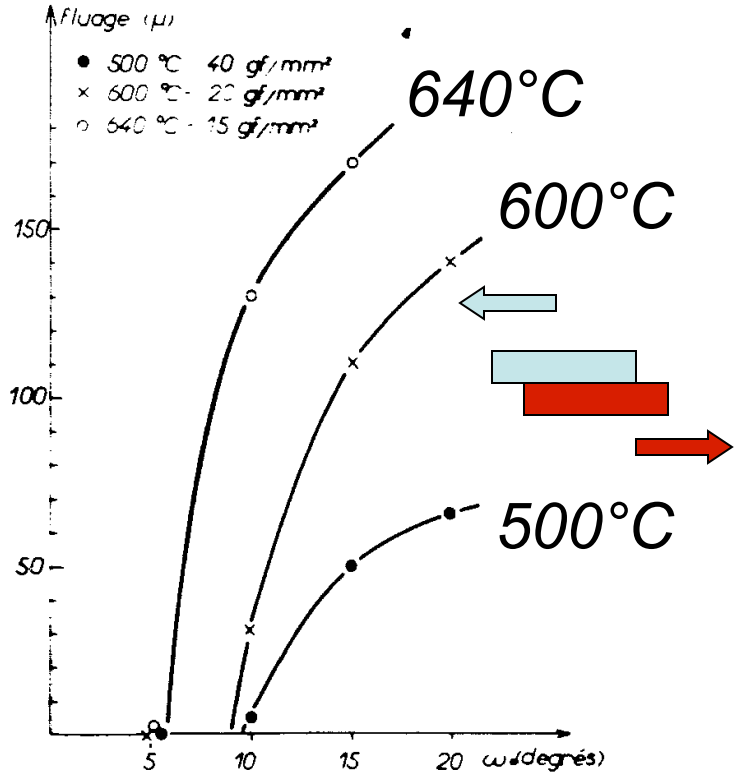

Fig. 23. — *Fluages mesurés au bout de* 100 mn, *dans diverses* ***conditions de*** *température et de charge, pour des joints de* ***faible désorientation.***

Biscondi, M. and C. Goux (1968), "Fluage intergranulaire de bicristaux orientés d'aluminium", *Mémoires Scientifiques Revue de Métallurgie* **55** 167-179.

Mobility: Overview

$$V = M\,\gamma\,\kappa$$

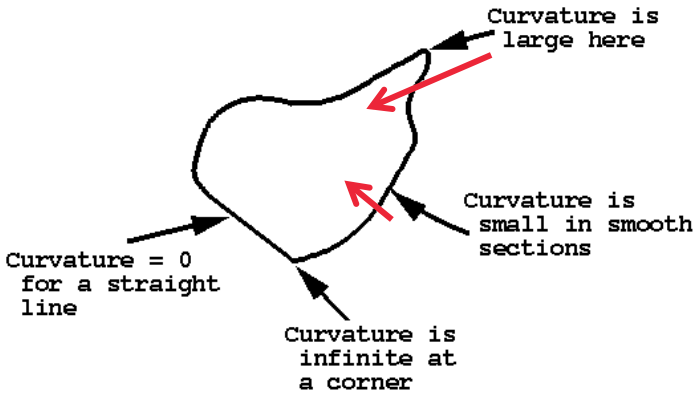

- Highest mobility observed for <111> tilt boundaries. At low temperatures, the *peaks* occur at a few CSL types - Σ7, especially.
- This behavior is inverse to that deduced from classical theory (Turnbull, Gleiter).
- For stored energy driving force, strong tilt-twist anisotropy observed.
- *No simple theory* available.
- Grain boundary mobilities and energies (anisotropy thereof) are essential for accurate modeling of evolution.

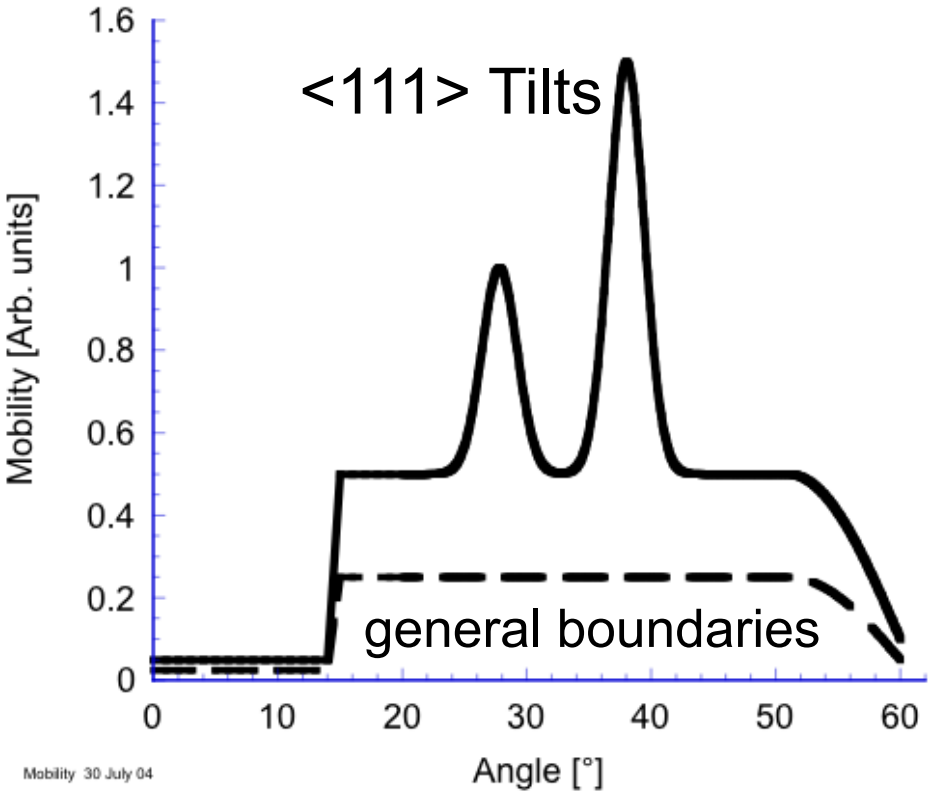

"Bridging Simulations and Experiments in Microstructure Evolution", Demirel *et al.*, *Phys. Rev. Lett.*, 90, 016106 (2003)
Grain Boundary Migration in Metals, G. Gottstein and L. Shvindlerman, CRC Press, 1999 (+ 2nd ed.).

Mobility vs. Boundary Type

Al+.03Zr - individual recrystallizing grains

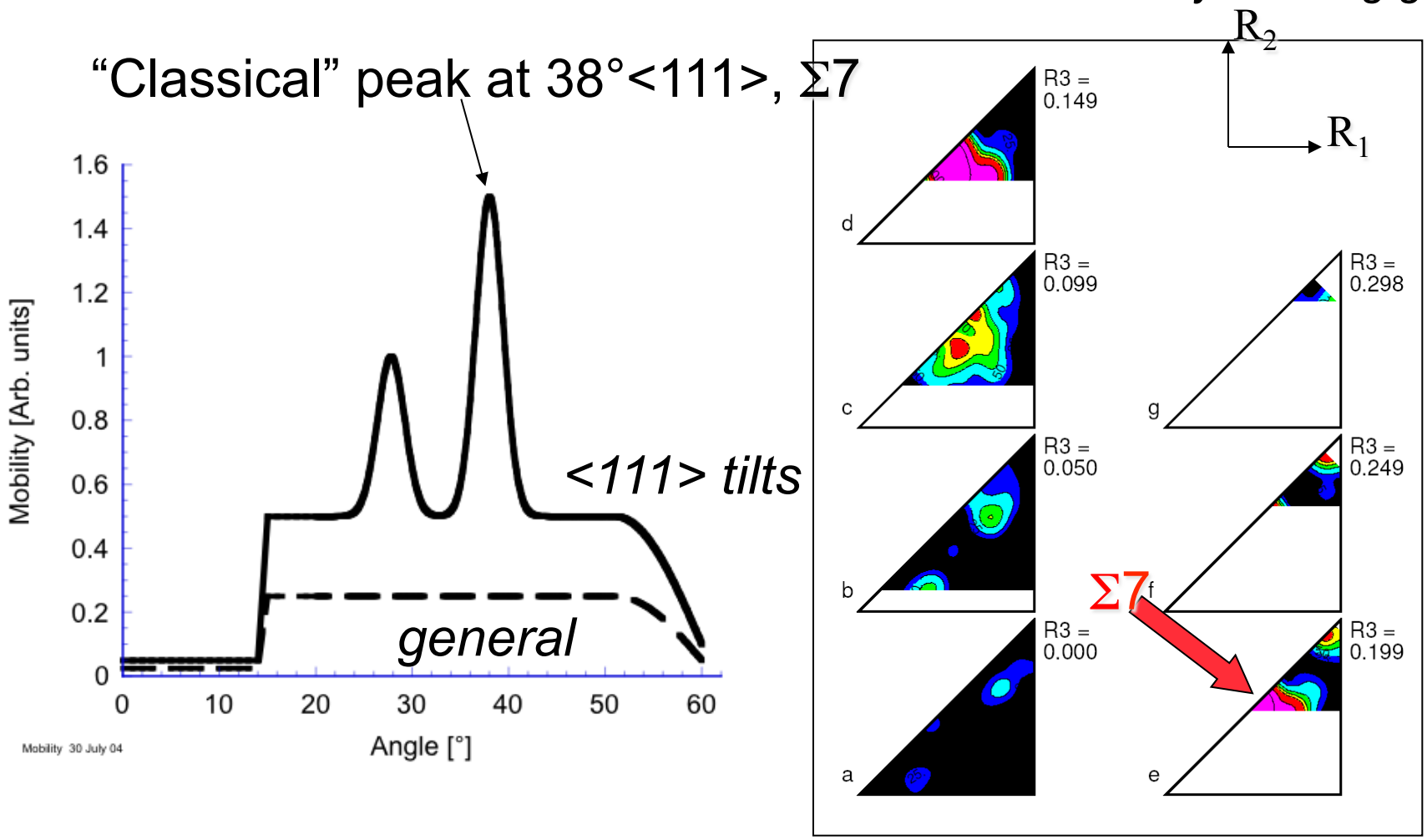

- At 350ºC, <u>only</u> boundaries close to 38°<111>, or Σ7 are mobile

Taheri et al. (2005) *Z. Metall.* **96** 1166

Grain Boundary Complexions

A Complexion Transitions is a change in grain boundary structure from one atomic structure (e.g. no impurities) to another (e.g. a bi-layer structure).

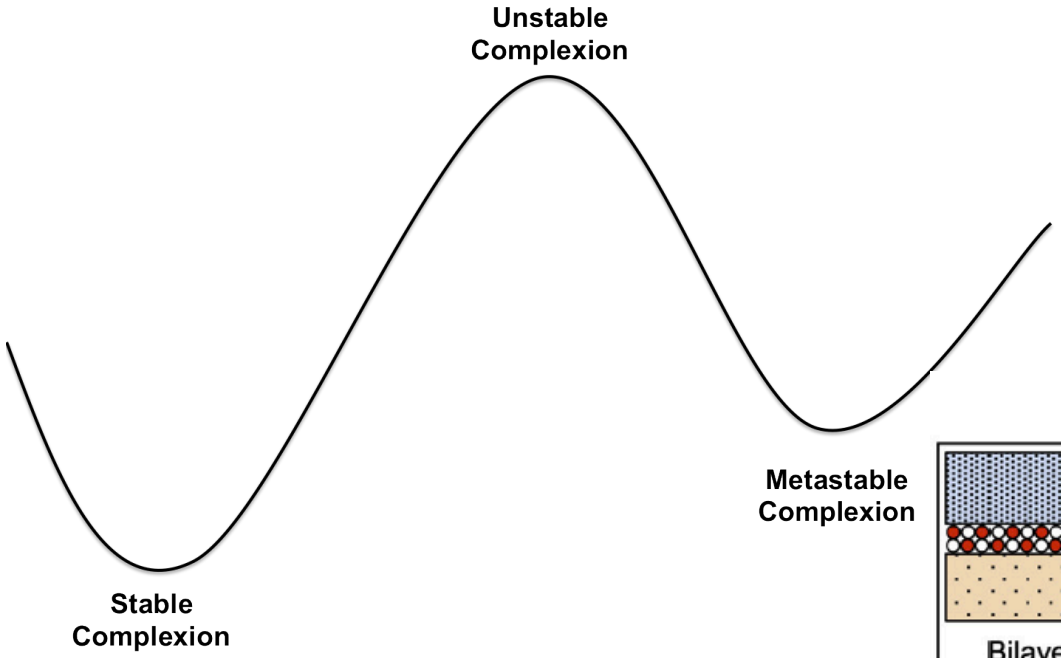

Complexion transitions occur when temperature and composition change such that one complexion becomes metastable with respect to another.

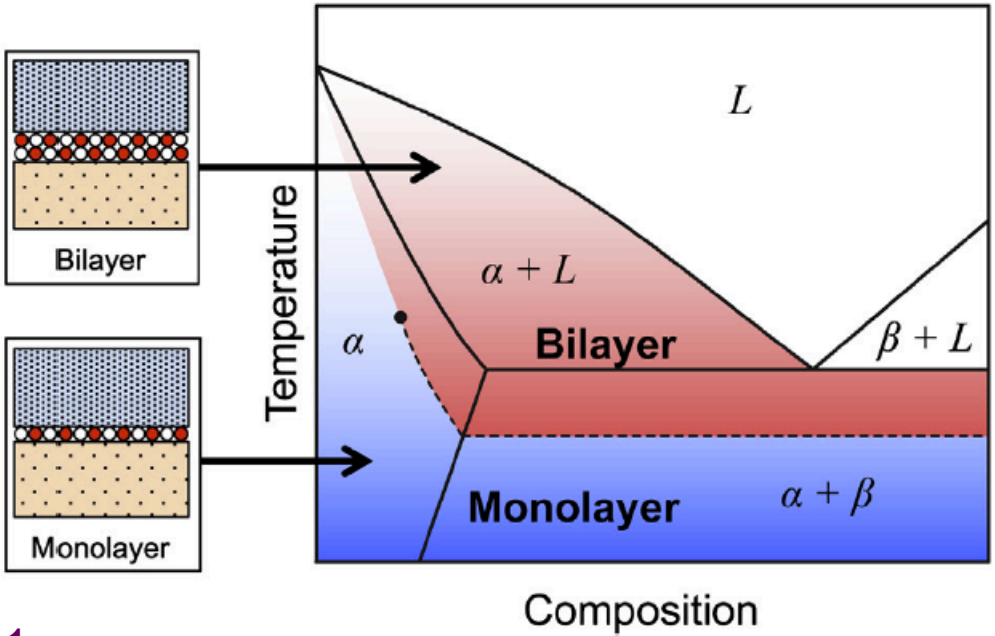

This often changes grain boundary properties, both energy and mobility

P.R. Cantwell *et al*. *Acta Mater*. (2014) **62** 1.

Complexion Transitions and AGG

Example: complexions in alumina with various dopants

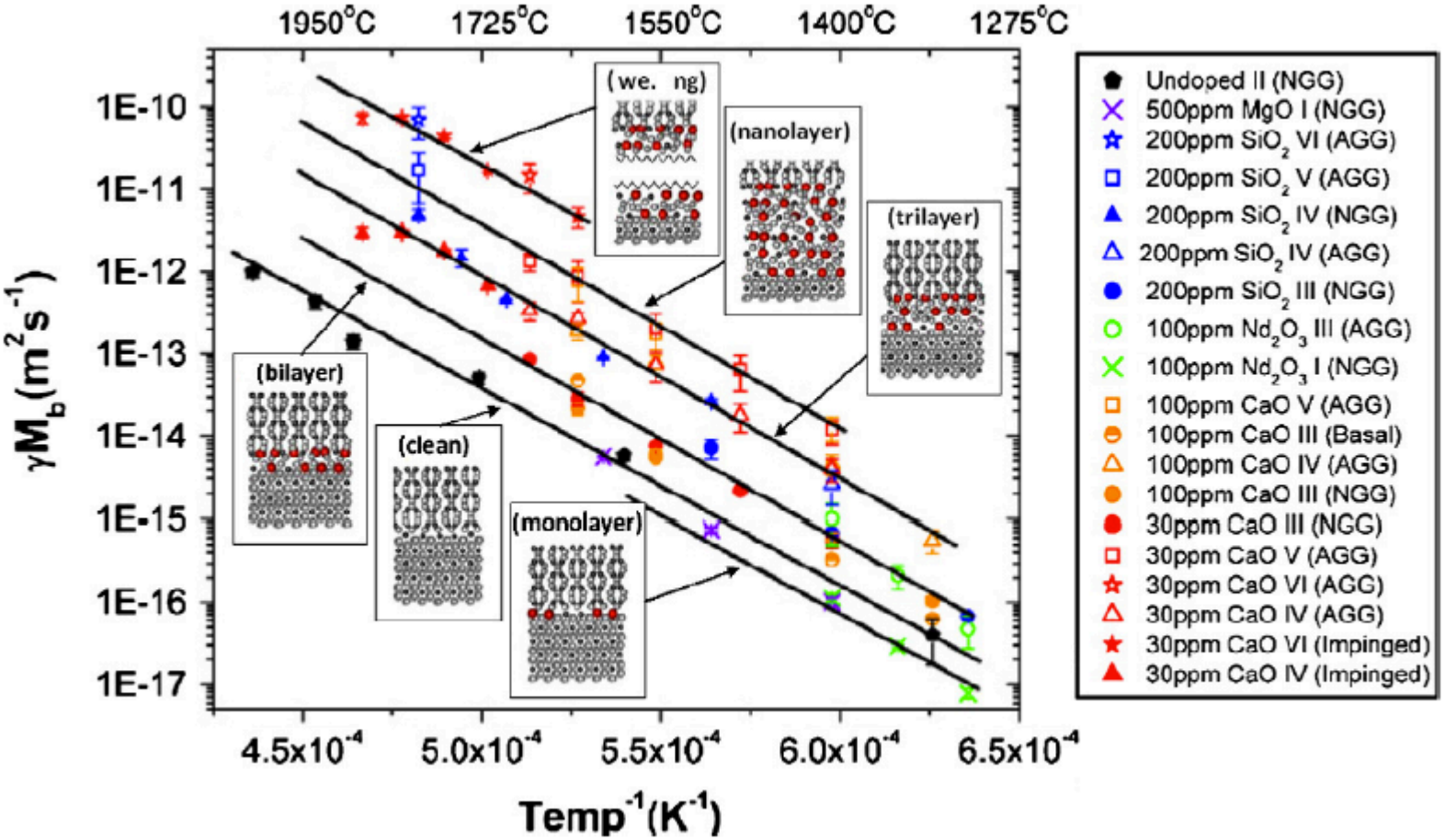

Grain boundary mobility increases as complexions get closer to complete wetting, but the slope with respect to temperature remains the same! Why?

S.J. Dillon *et al*. *J. Amer. Ceram. Soc*. (2008) **91** 2304.

Complexion Transitions and AGG

Implication: many grain boundaries changed complexion AFTER coming into contact with abnormal grains!

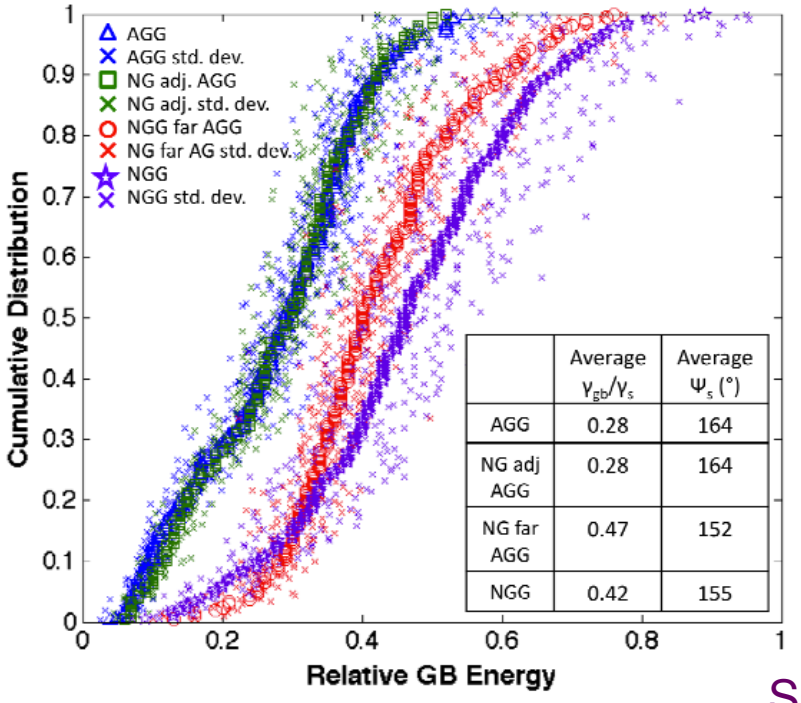

	Average γ_{gb}/γ_s	Average Ψ_s (°)
AGG	0.28	164
NG adj AGG	0.28	164
NG far AGG	0.47	152
NGG	0.42	155

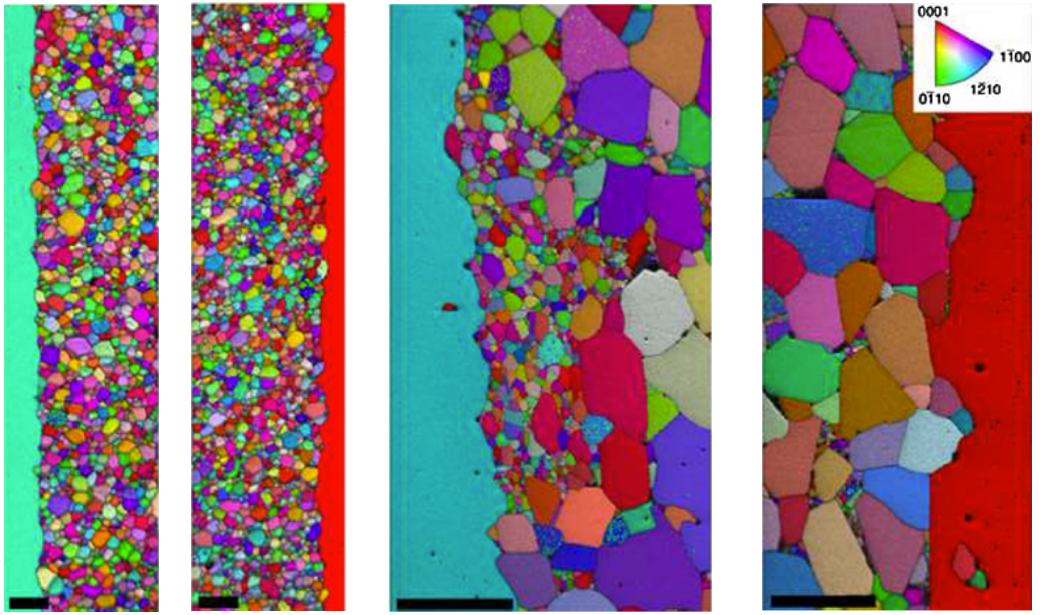

S.A. Bojarski *et al.*, *Mater. Sci. Forum* (2013) **753** 87

S.A. Bojarski *et al*. *Metall. and Mater. Trans. A* (2012) **43** 3532

Grain Boundary Energy: Definition

- Grain boundary energy is defined as the excess free energy associated with the presence of a grain boundary, with the perfect lattice as the reference point.
- A thought experiment provides a means of quantifying GB energy, γ. Take a patch of boundary with area A, and increase its area by dA. The grain boundary energy is the proportionality constant between the increment in total system energy and the increment in area. This we write as:

$$\gamma = dG/dA$$

- The physical reason for the existence of a (positive) GB energy is misfit between atoms across the boundary. The deviation of atom positions from the perfect lattice leads to a higher energy state. Wolf established that GB energy is correlated with excess volume in an interface. There is no simple method, however, for predicting the excess volume based on a knowledge of the grain boundary crystallography.

Grain boundary energy, γ: overview

- Grain boundary energies can be extracted from 3D images by measurement of dihedral angles at triple lines and by exploiting the Herring equations at triple junctions.
- The population of grain boundaries are **inversely correlated** with grain boundary energy.
- Apart from a few deep cusps, the relative grain boundary energy varies over a small range, ~ 40%.
- The grain boundary energy scales with the excess volume; unfortunately no model exists to connect excess volume with crystallographic type.
- The **average of the two surface energies** has been demonstrated to be highly correlated with the **grain boundary energy** in MgO.
- For metals, population statistics suggest that a few deep cusps in energy exist for both CSL-related and non-CSL boundary types (e.g. in fcc, Σ3, Σ11), based on both experiments and simulation.
- Theoretical values of grain boundary energy have been computed by a group at Sandia Labs (Olmsted, Foiles, Holm) using molecular statics, and GB mobilities using molecular dynamics.

Olmsted *et al*. (2009) "… Grain boundary energies" *Acta mater.* **57** 3694;
Rohrer, *et al*. (2010) "Comparing … energies." *Acta mater.* **58** 5063; Holm *et al*., *Acta mater.* **59** 5250

G.B. Properties Overview: Energy

- Low angle boundaries can be treated as dislocation structures, as analyzed by Read & Shockley (1951).
- Grain boundary energy can be constructed as the average of the two surface energies - $\gamma_{GB} = \gamma(hkl_A)+\gamma(hkl_B)$.
- For example, in *fcc* metals, low energy boundaries are found with {111} terminating surfaces.
- In most *fcc* metals, certain CSL types are much more common than expected from a random texture.
- Does mobility scale with g.b. energy, based on a dependence on acceptor/ donor sites? Answer: this supposition is *not* valid.

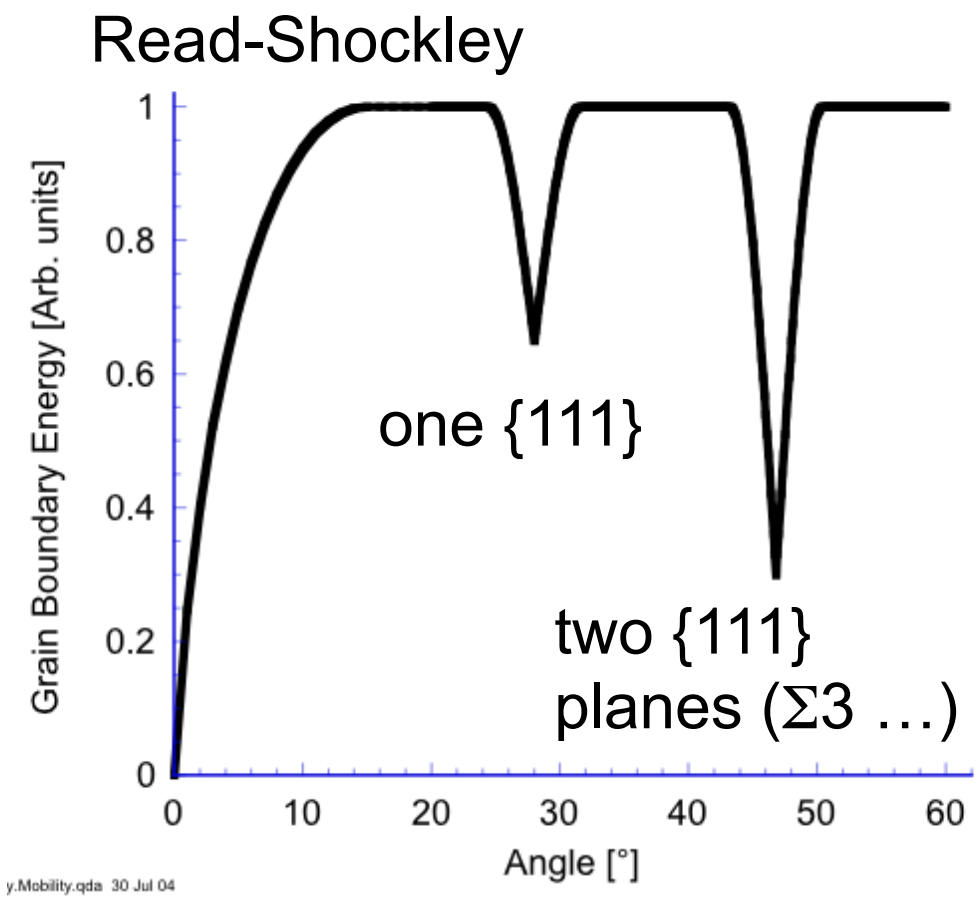

Shockley W., Read W.T., "Quantitative Predictions From Dislocation Models Of Crystal Grain Boundaries." *Phys. Rev.* (1949) **75** 692.

Grain Boundary Energy

- First categorization of boundary type is into *low-angle* versus *high-angle* boundaries. Typical value in cubic materials is 15° for the misorientation angle.
- Typical values of average grain boundary energies vary from 0.32 $J.m^{-2}$ for Al to 0.87 for Ni $J.m^{-2}$ (related to bond strength, which is related to melting point).
- Read-Shockley model describes the energy variation with angle for *low-angle boundaries* successfully in many experimental cases, based on a dislocation structure.

Read-Shockley model

Read-Shockley applies to Low Angle Grain Boundaries (LAGB)

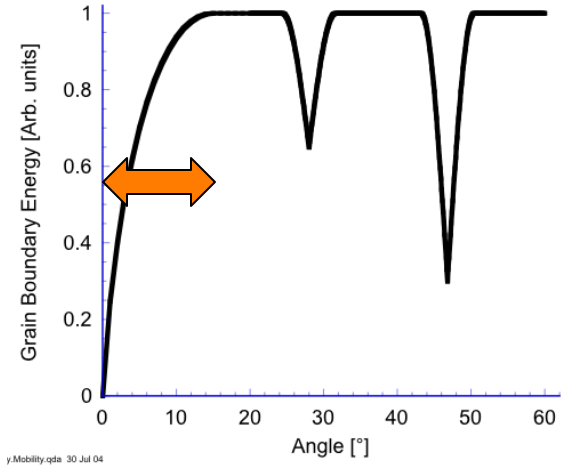

- Start with a symmetric tilt boundary composed of a wall of infinitely straight, parallel edge dislocations (e.g. based on a 100, 111 or 110 rotation axis with the planes symmetrically disposed).
- Dislocation density (L^{-1}) given by:

$1/D = 2\sin(\theta/2)/b \approx \theta/b$ for small angles.

Tilt boundary

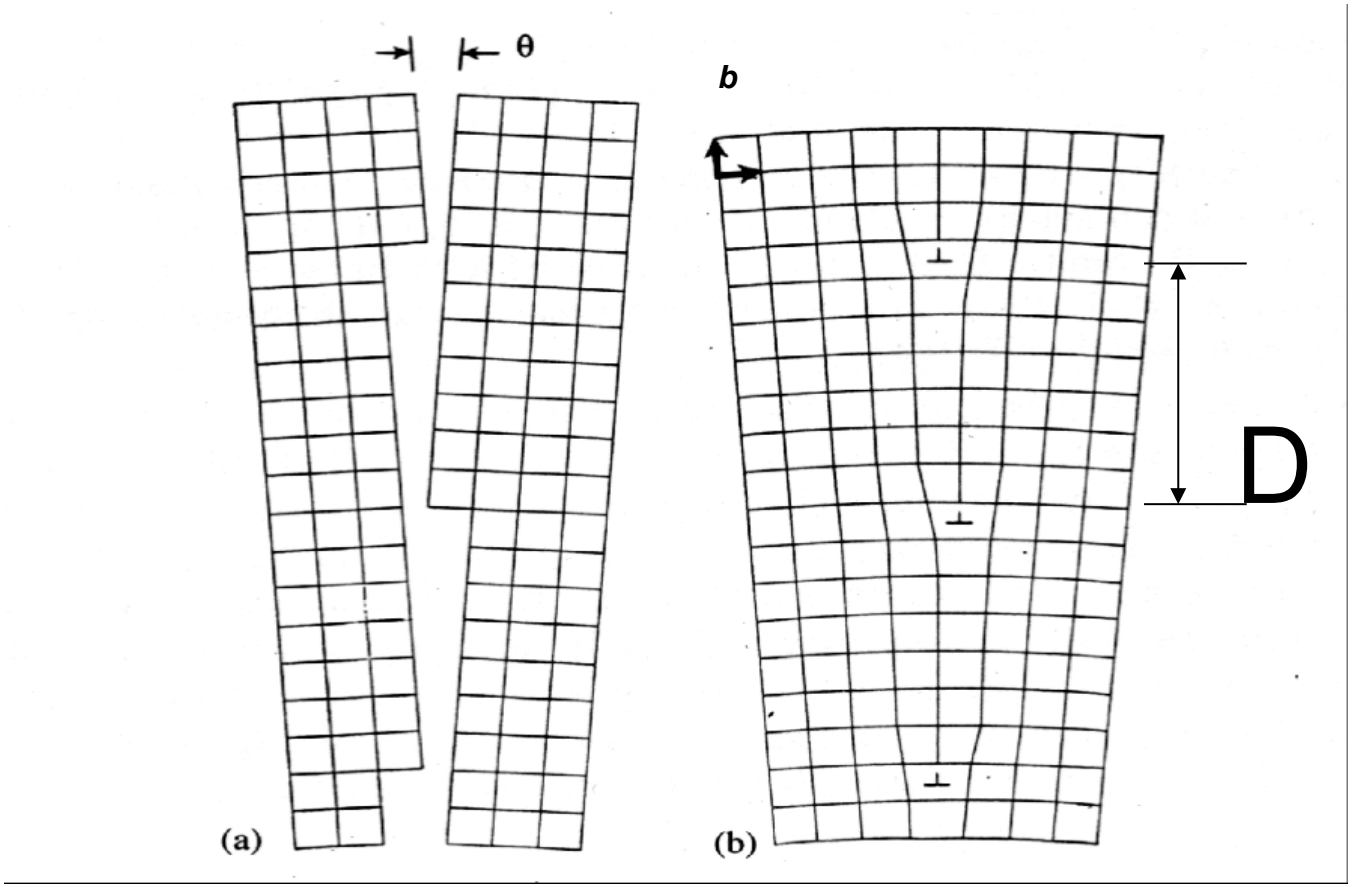

Each dislocation accommodates the mismatch between the two lattices; for a <112> or <111> misorientation axis in the boundary plane, only one type of dislocation (a single Burgers vector) is required.

Read-Shockley model, contd.

- For an infinite array of edge dislocations the long-range stress field depends on the spacing. Therefore given the dislocation density and the core energy of the dislocations, the energy of the wall (boundary) is estimated (r_0 sets the core energy of the dislocation):

$$\gamma_{gb} = E_0\,\theta\,(A_0 - \ln\theta), \text{ where}$$

$$E_0 = \mu b/4\pi(1-\nu);\;\; A_0 = 1 + ln(b/2\pi r_0)$$

- Note that differentiation of the Eq above leads to a maximum energy when $exp(\theta) = (A_0 - 1)$, or, $\theta = b/2\pi r_0$, which shows that the choice of the cut-off radius, r_0, determines the maximum in the energy.

Read-Shockley model, contd.

- If the non-linear form for the dislocation spacing is used, we obtain a sine-law variation (U_{core}= core energy):

$$\gamma_{gb} = \sin|\theta| \{U_{core}/b - \mu b^2/4\pi(1-\nu) \ln(\sin|\theta|)\}$$

- Note: this form of energy variation may also be applied to CSL-vicinal boundaries.

LAGB experimental results

- Experimental results on copper. Note the lack of evidence of deep minima (cusps) in energy at CSL boundary types in the <001> tilt or twist boundaries. Also note that the sine curve appears to apply over the entire angular range, not just up to 15°.

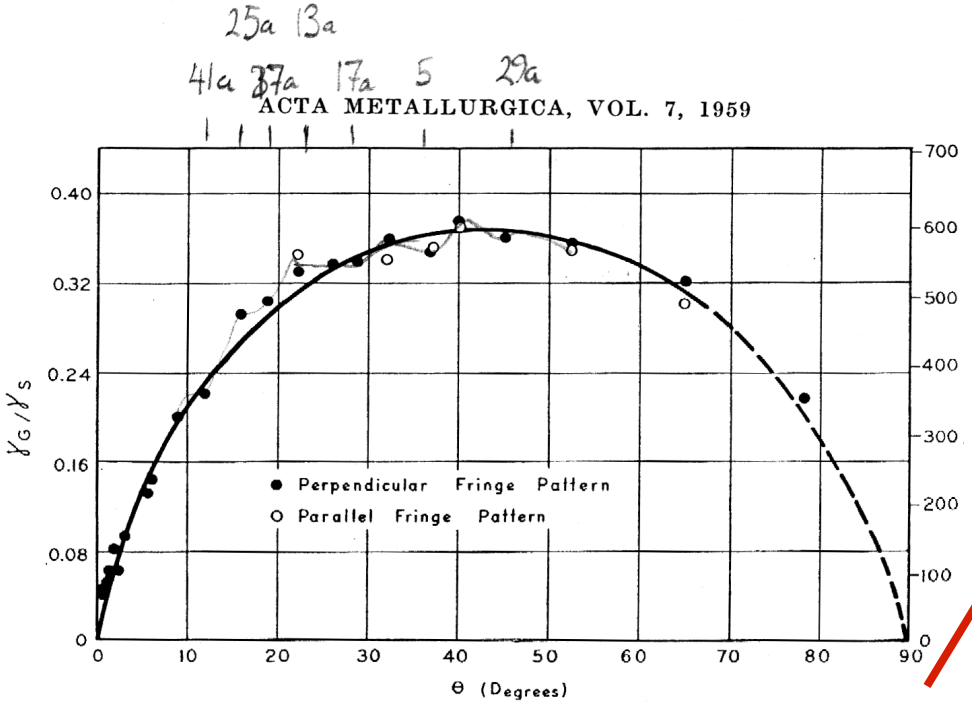

FIG. 4. Dependence of grain boundary energy on misorientation for [001] tilt boundaries at 1065°C. Solid line represents the curve calculated from equation (1), using the *large angle parameters*. Although the curve has no theoretical significance it can be used as an empirical representation of the energy data over the range $5° < \theta < 43°$. Beyond 43°, the curve has been drawn to fit the experimental points.

Disordered Structure

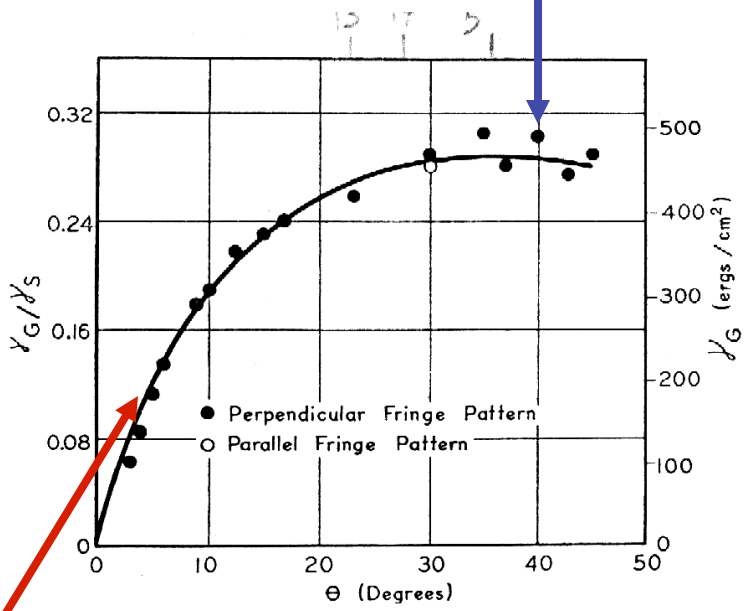

FIG. 5. Dependence of grain boundary energy on misorientation for [001] twist boundaries at 1065°C. The curve was calculated from equation (1), using the *large angle parameters*, and therefore it has no theoretical significance, but it can be used to represent the experimental points.

Dislocation Structure

Gjostein & Rhines, *Acta metall.* **7**, 319 (1959)

Physical Meaning of 5 Macroscopic Grain Boundary Parameters

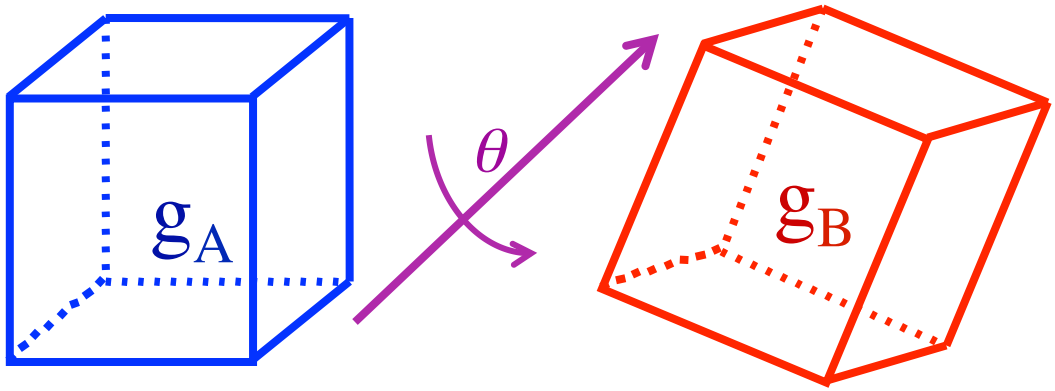

Lattice Misorientation, Δg (rotation, 3 parameters)

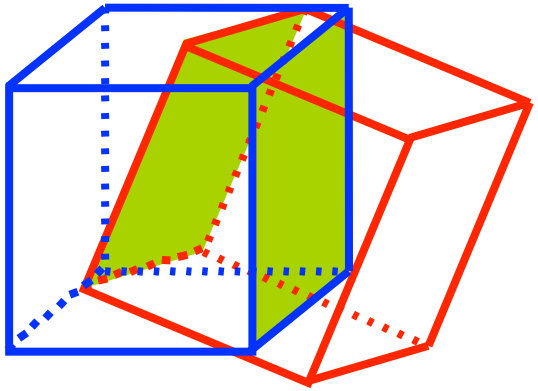

Boundary Plane Normal, $\mathbf{n}$ (unit vector, 2 parameters)

Grain Boundaries have 5 Macroscopic Degrees of Freedom

Measurement of GB Energy

- We need to be able to measure grain boundary energy.
- In general, we do not need to know the absolute value of the energy but only how it varies with boundary type, i.e. with the crystallographic nature of the boundary.
- For measurement of the anisotropy of the energy, then, we rely on local equilibrium at junctions between boundaries. This can be thought of as a force balance at the junctions.
- For not too extreme anisotropies, the junctions always occur as triple lines.

Experimental Methods for g.b. energy measurement

G. Gottstein & L. Shvindlerman, *Grain Boundary Migration in Metals*, CRC (1999)

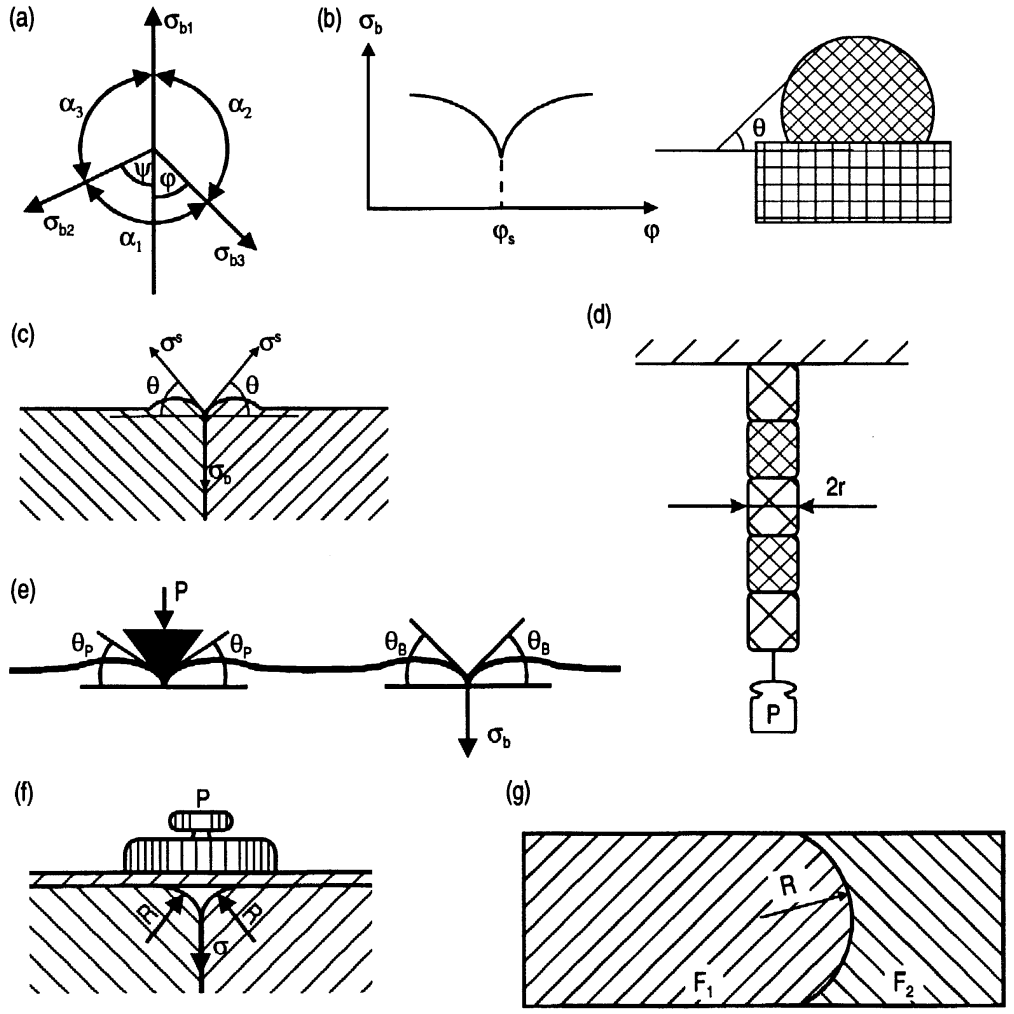

Fig. 1.9. Methods of grain boundary surface tension measurement: (a) – equilibrium angles at triple function; (b) – rotating ball method: sintering of small signal crystal balls to single crystal substrate; (c) – thermal groove method, (d) – zero creep method; (e) – method of a "floating" wedge; (f) – hypothetical method of an "equilibrium" grain boundary thermal groove; (g) – balance of grain boundary surface tension and volume diving force.

Method (a), with dihedral angles at triple lines, is most generally useful; method (b), with surface grooving also used.

Herring Equations

- We can demonstrate the effect of interfacial energies at the (triple) junctions of boundaries.
- Equal g.b. energies on 3 GBs implies equal dihedral angles:

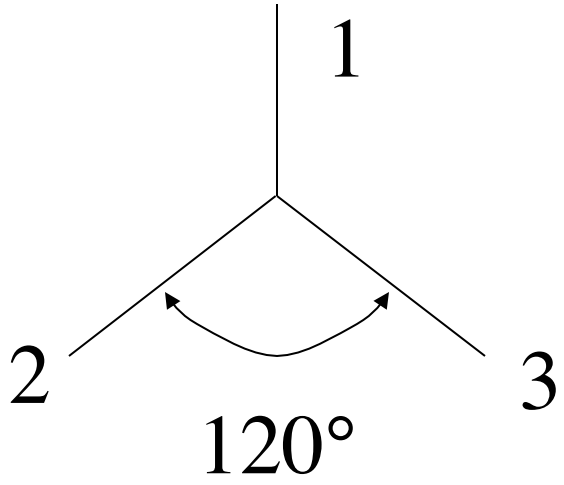

$\gamma_1 = \gamma_2 = \gamma_3$

Definition of Dihedral Angle

- Dihedral angle, χ:= angle between the tangents to an adjacent pair of boundaries (unsigned). In a triple junction, the dihedral angle is assigned to the opposing boundary.

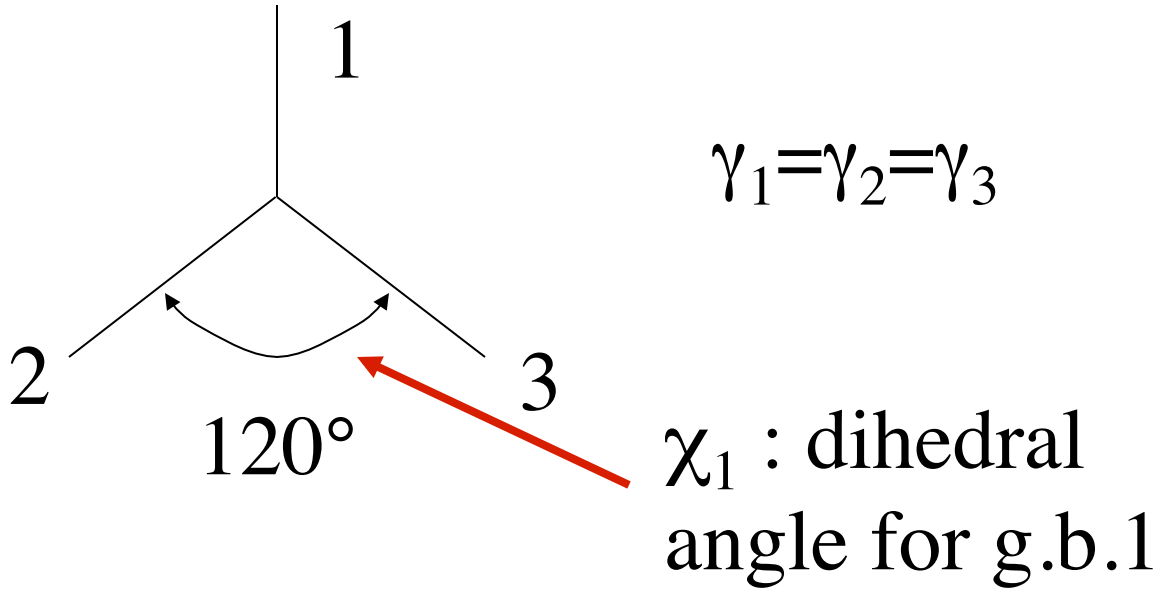

Dihedral Angles

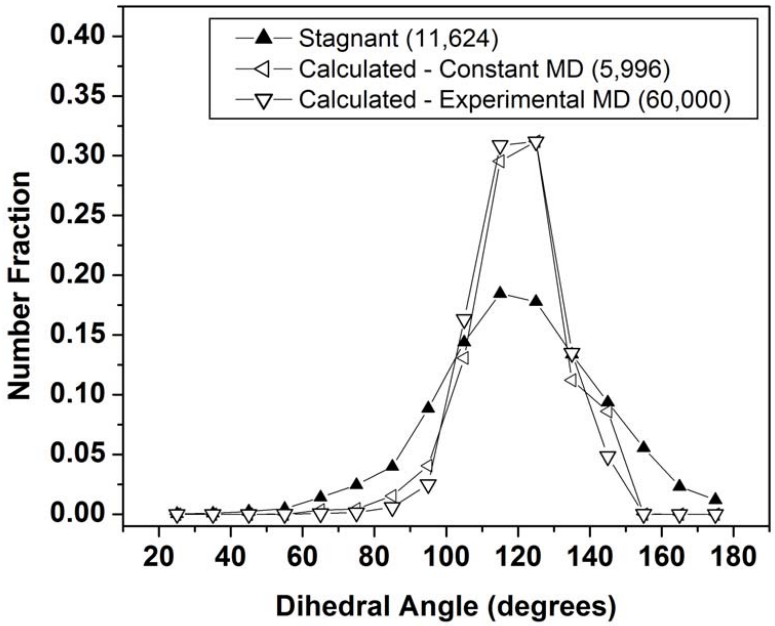

- An material with uniform grain boundary energy should have dihedral angles equal to 120°.
- Likely in real materials? No! Low angle boundaries (crystalline materials) always have a dislocation structure and therefore a monotonic increase in energy with misorientation angle (Read-Shockley model).
- The inset figure is taken from Barmak et al. *Progr. Matls. Sci*. **58** 987 (2013) and shows the distribution of dihedral angles measured in a 0.1 μm thick film of Al, along with a calculated distribution based on an GB energy function from a similar film (with two different assumptions about the distribution of misorientations). Note that the measured dihedral angles have a wider distribution than the calculated ones.

Unequal energies

- If the interfacial energies are not equal, then the dihedral angles change. A low g.b. energy on boundary 1 *increases* the corresponding dihedral angle.

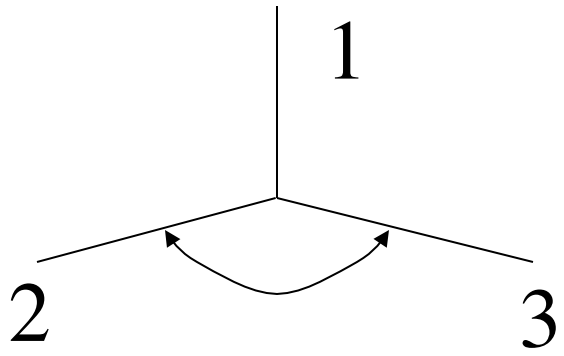

$\gamma_1 < \gamma_2 = \gamma_3$

$\chi_1 > 120°$

Unequal Energies, contd.

- A high g.b. energy on boundary 1 *decreases* the corresponding dihedral angle.
- Note that the dihedral angles depend on *all* the energies.

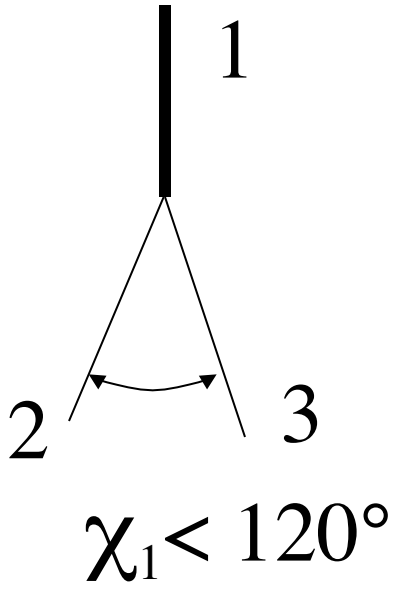

$\gamma_1 > \gamma_2 = \gamma_3$

See Fisher & Fullman *JAP* **22** 1350 (1951) for application to analysis of annealing twin formation.

Wetting

- For a large enough ratio, wetting can occur, i.e. replacement of one boundary by the other two at the TJ.

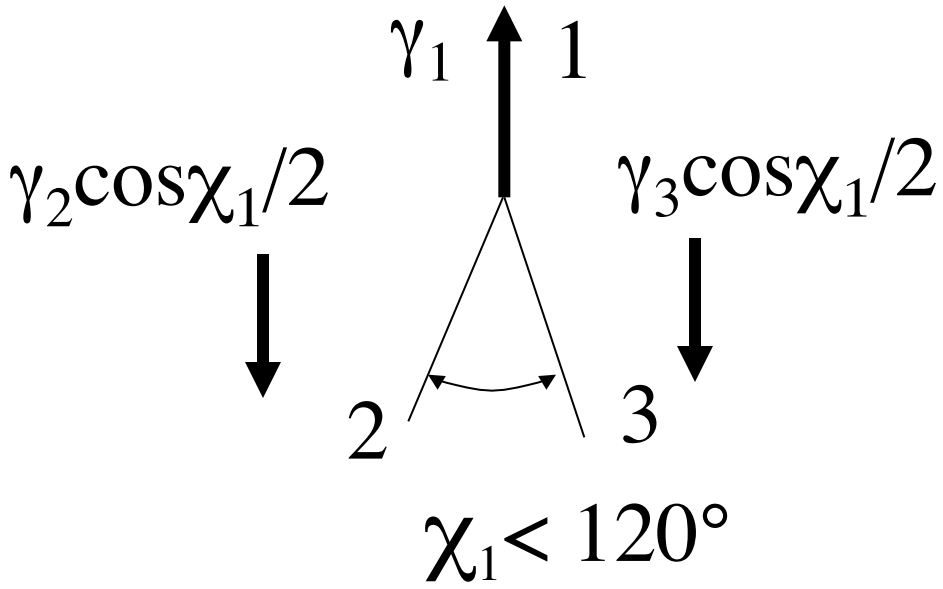

$\gamma_1 > \gamma_2 = \gamma_3$

Balance vertical forces $\Rightarrow$

$\gamma_1 = 2\gamma_2 \cos(\chi_1/2)$

Wetting $\Rightarrow$

$\gamma_1 \geq 2\,\gamma_2$

Triple Junction Quantities

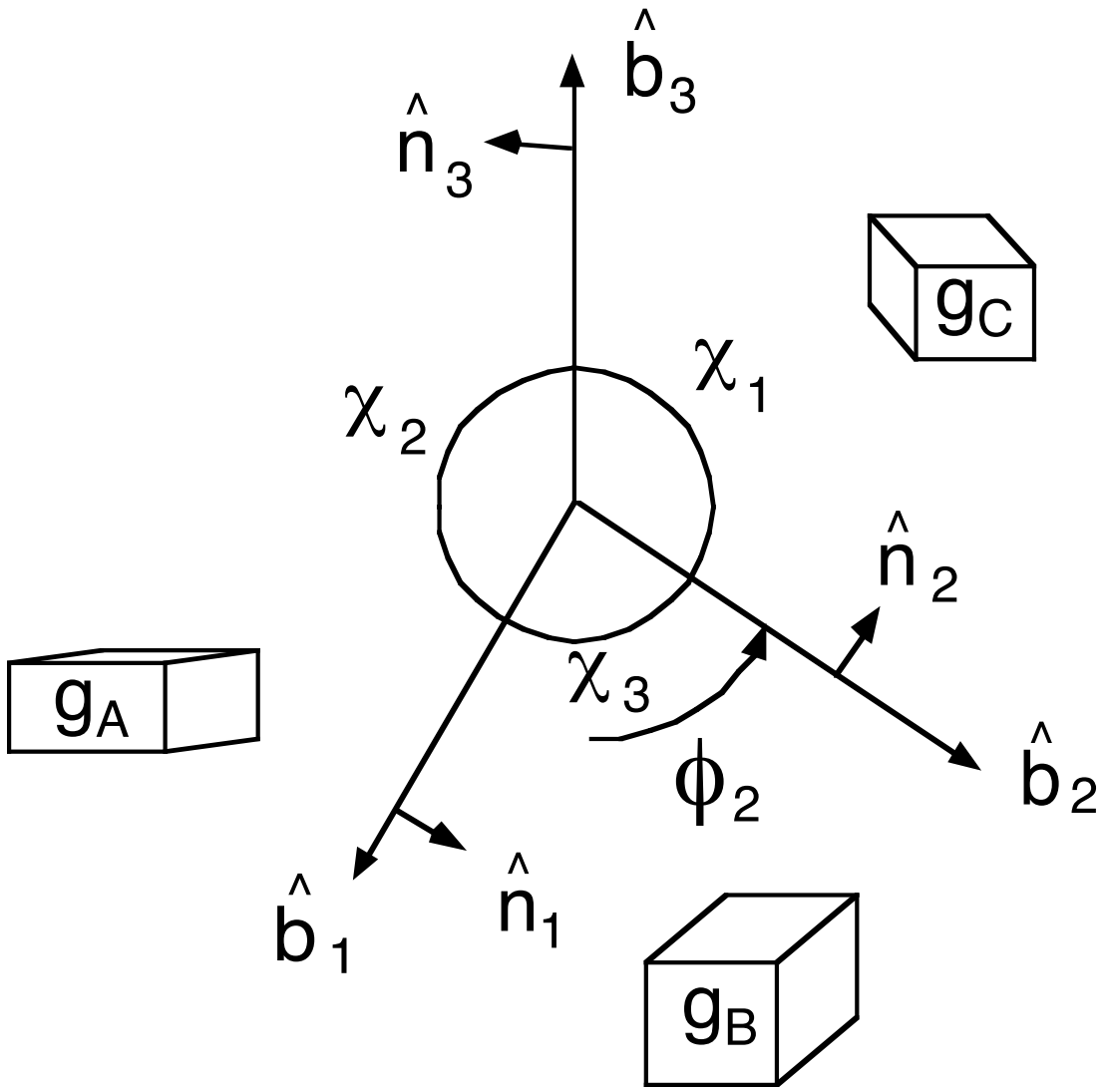

Triple Junction Quantities

- Grain boundary tangent (at a TJ): **b**
- Grain boundary normal (at a TJ): **n**
- Grain boundary inclination, measured anti-clockwise with respect to a(n arbitrarily chosen) reference direction (at a TJ): ϕ
- Grain boundary dihedral angle: χ
- Grain orientation:*g*

Force Balance Equations/ Herring Equations

- The Herring equations [(1951). Surface tension as a motivation for sintering. The Physics of Powder Metallurgy. New York, McGraw-Hill Book Co.**:** 143-179] are force balance equations at a TJ. They rely on a *local equilibrium* in terms of free energy.
- A virtual displacement, $\delta\mathbf{r}$, of the TJ (*L* in the figure) results in no change in free energy.
- See also: Adams *et al*., *Interface Science* **7** 321 (1999); Kinderlehrer D and Liu C, *Mathematical Models and Methods in Applied Sciences*, (2001) **11** 713-729; Kinderlehrer, *et al*. (2004) "Mesoscale simulation of grain growth", in *Continuum Scale Simulation of Engineering Materials*, (Raabe, D. *et al*., eds),Wiley-VCH Verlag, Weinheim, Chap. 16, 361-372

Derivation of Herring Equs.

A virtual displacement, $\delta\mathbf{r}$, of the TJ results in no change in free energy.

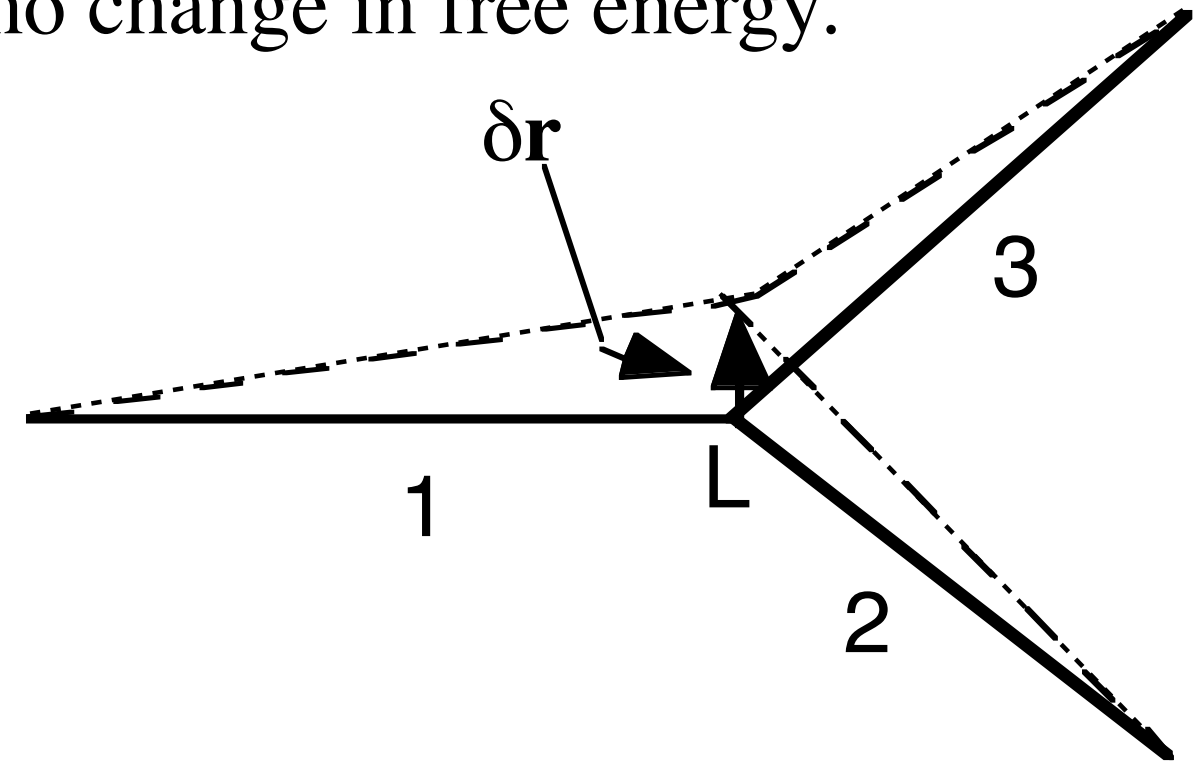

See also: Adams et al., *Interface Science* **7** 321 (1999); Kinderlehrer, D and Liu, C *Mathematical Models and Methods in Applied Sciences* (2001) **11** 713; Kinderlehrer et al. (2004) Mesoscale simulation of grain growth, in Continuum Scale Simulation of Engineering Materials, (Raabe, D. et al., eds), Wiley-VCH Verlag, Weinheim, Chapt. 16, p361.

Force Balance

- Consider only interfacial energy: vector sum of the forces must be zero to satisfy equilibrium. Each "**b**" is a tangent (unit) vector.

$$\gamma_1 \mathbf{b}_1 + \gamma_2 \mathbf{b}_2 + \gamma_3 \mathbf{b}_3 = \vec{0}$$

- These equations can be rearranged to give the Young equations *(sine law):*

$$\frac{\gamma_1}{\sin \chi_1} = \frac{\gamma_2}{\sin \chi_2} = \frac{\gamma_3}{\sin \chi_3}$$

Analysis of Thermal Grooves to obtain GB Energy

See, for example: Gjostein, N. A. and F. N. Rhines (1959). "Absolute interfacial energies of [001] tilt and twist grain boundaries in copper." Acta metall. 7 319

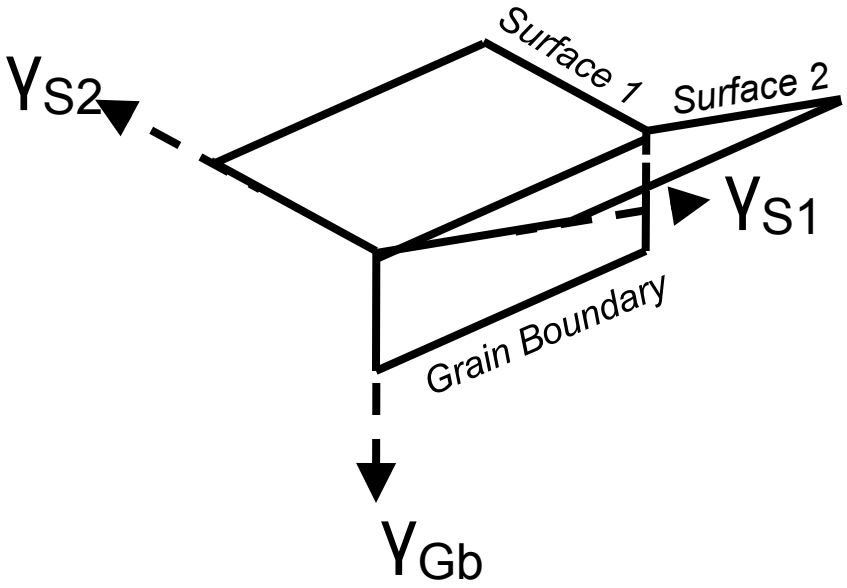

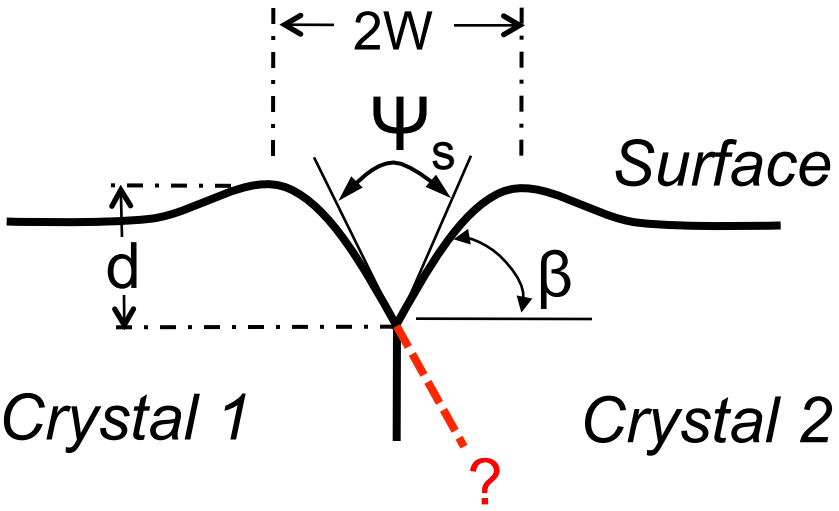

$$\frac{W}{d} = \frac{4.73}{\tan\beta}$$

$$\frac{\gamma_{Gb}}{\gamma_S} = 2Cos\left(\frac{\Psi_S}{2}\right)$$

It is often reasonable to assume a constant surface energy, γ_S, and examine the variation in GB energy, γ_{Gb}, as it affects the thermal groove angles

Grain Boundary Energy Distribution is Affected by Alloying

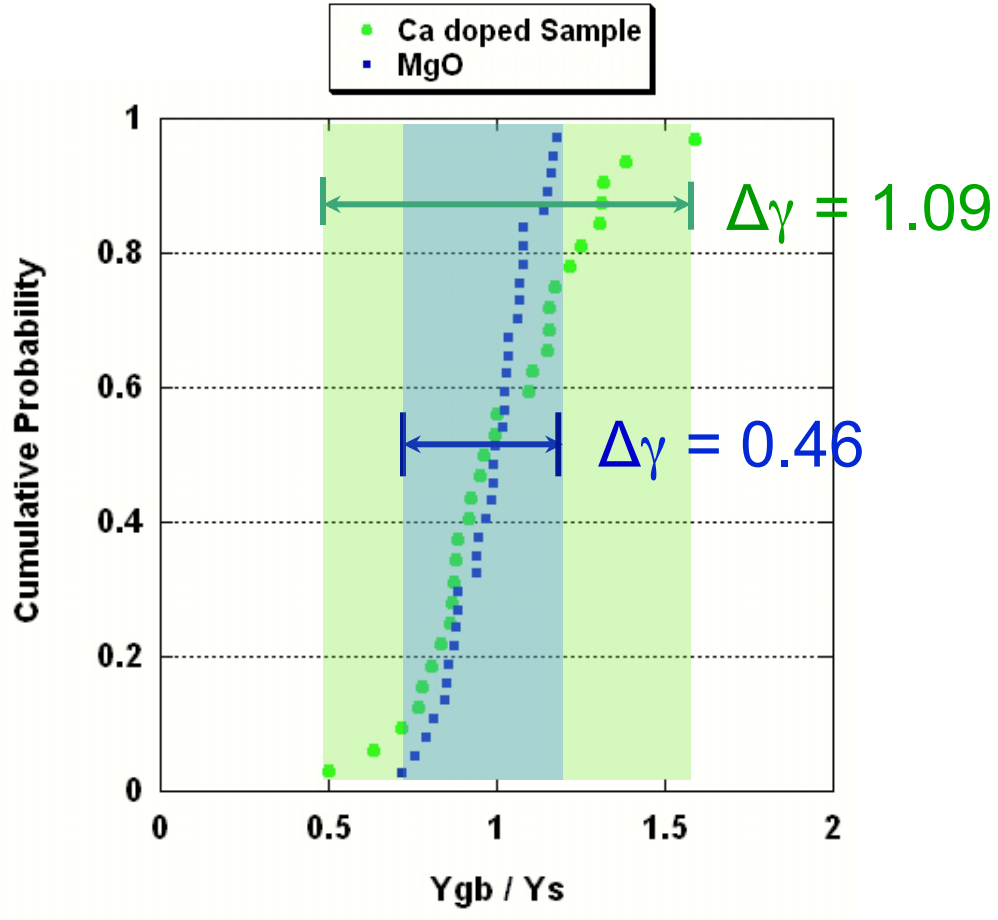

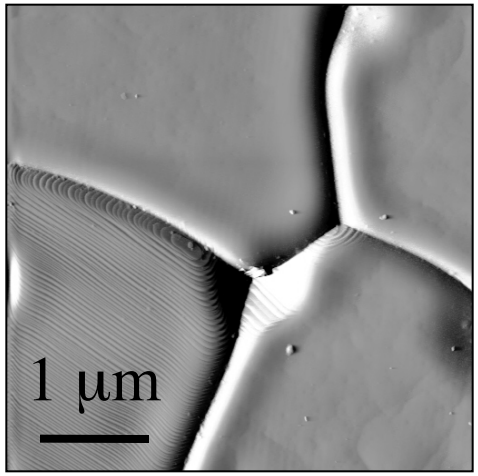

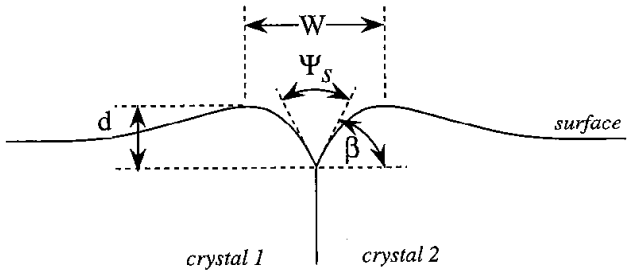

$$\frac{\gamma_{gb}}{\gamma_s} = 2\cos\frac{\psi_s}{2}$$

Ca solute increases the range of the γ_{GB}/γ_S ratio. The variation of the relative energy in doped MgO is higher (broader distribution) than in the case of undoped material.

Bi impurities in Ni have the opposite effect

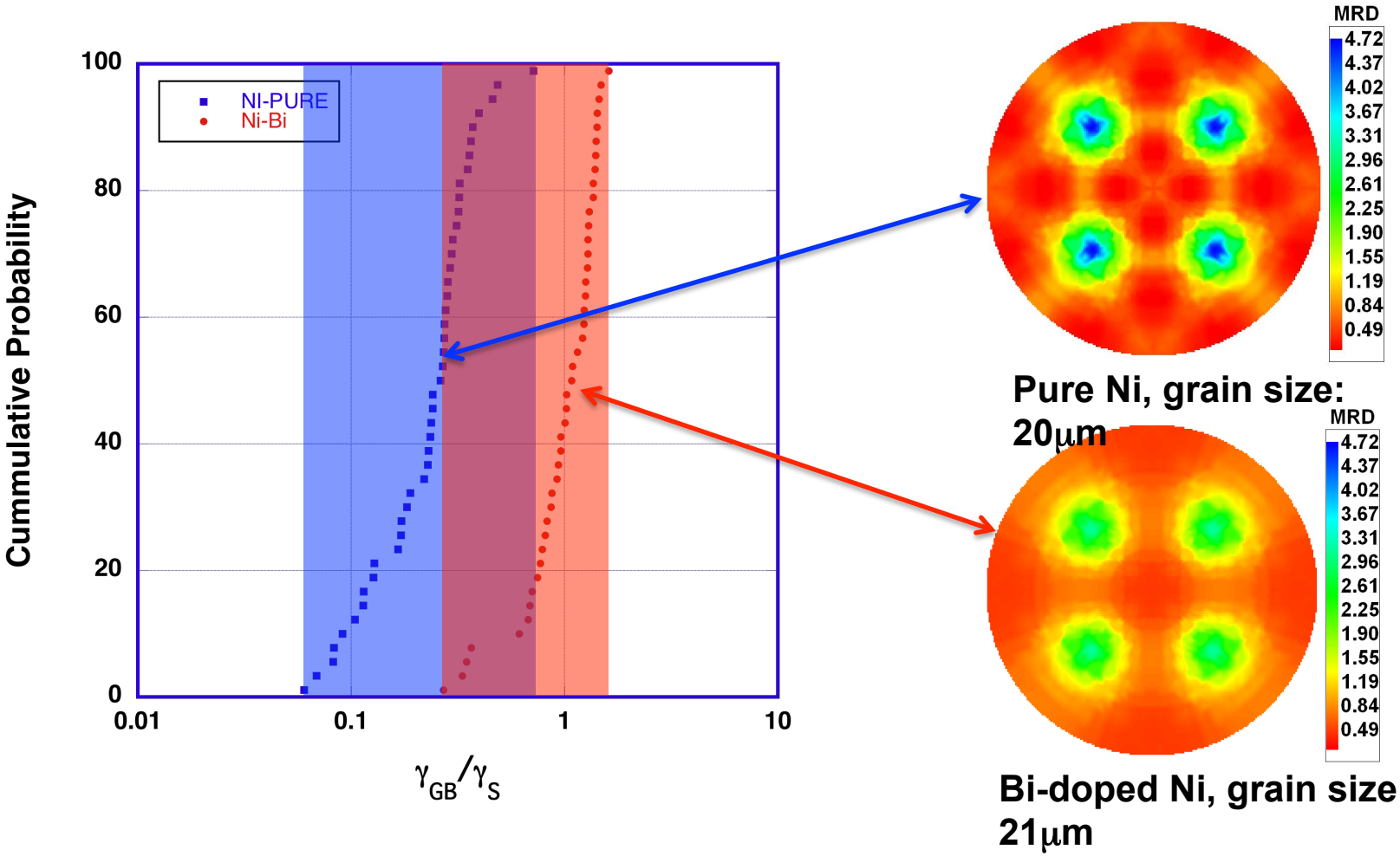

Range of γ_{GB}/γ_S (on log scale) is smaller for Bi-doped Ni than for pure Ni, indicating **smaller** anisotropy of γ_{GB}/γ_S. This correlates with the plane distribution.

Separation of Δg and **n**

Plotting the boundary plane requires a full hemisphere which projects as a circle. Each projection describes the variation at fixed misorientation. Any (numerically) convenient discretization of misorientation and boundary plane space can be used.

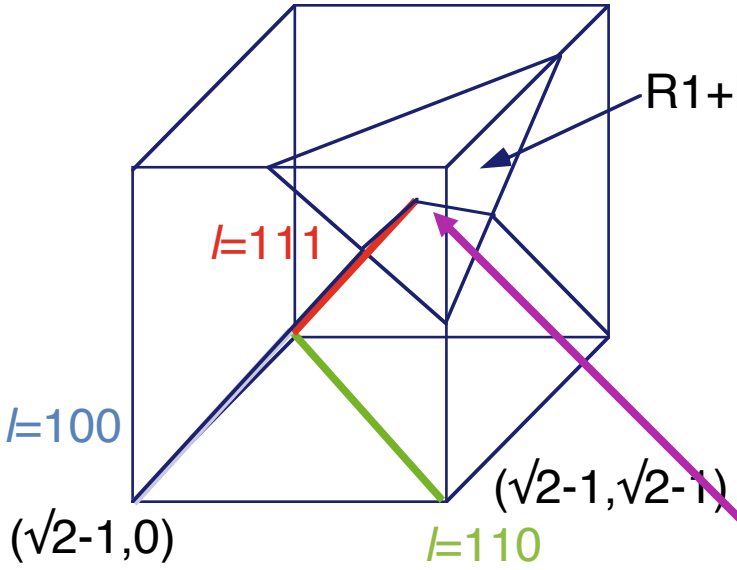

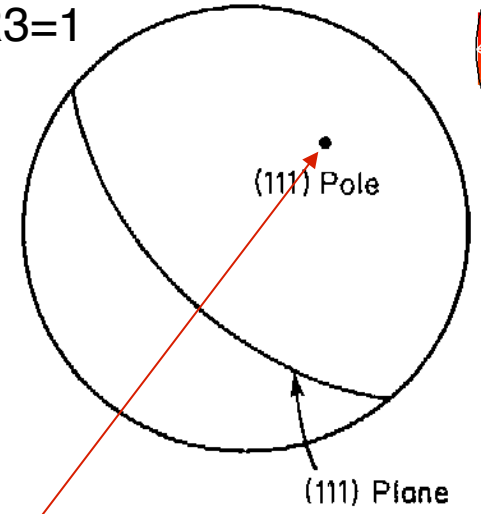

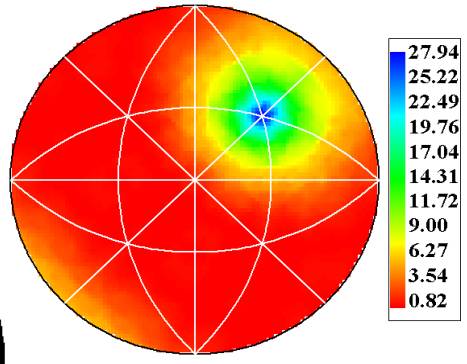

Distribution of normals for boundaries with Σ3 misorientation (commercial purity Al)

Misorientation axis, e.g. 111, also the twist type location

Tilt versus Twist Boundaries

Isolated/occluded grain (one grain enclosed within another) illustrates variation in boundary plane for constant misorientation. The normal is // misorientation axis for a twist boundary whereas for a tilt boundary, the normal is ⊥ to the misorientation axis. Many variations are possible for any given boundary.

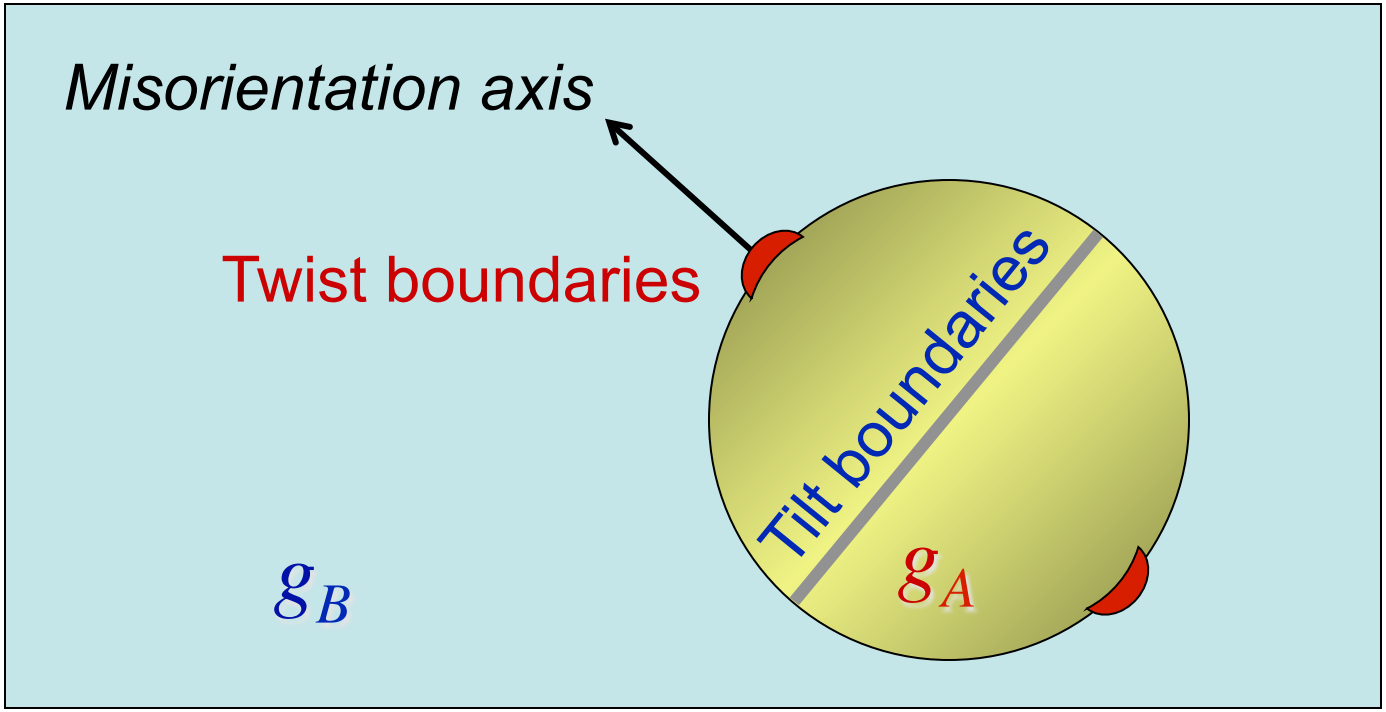

Inclination Dependence

- Interfacial energy can depend on *inclination*, i.e. which crystallographic plane is involved.
- Example? The coherent twin boundary is obviously low energy as compared to the incoherent twin boundary (e.g. Cu, Ag). The misorientation (60° about <111>) is the same, so *inclination* is the only difference.

Twin: coherent vs. incoherent

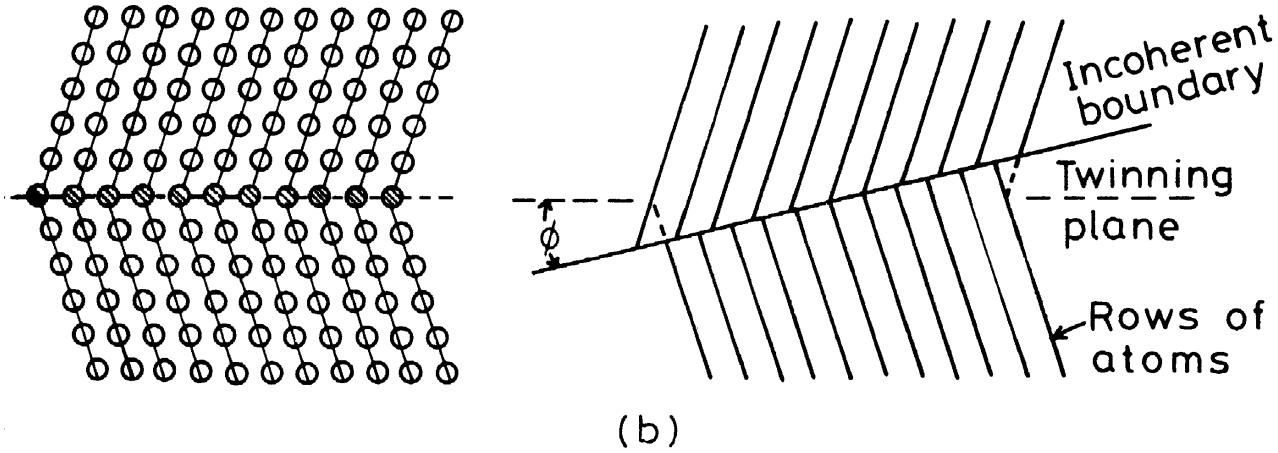

- Porter & Easterling fig. 3.12/ p123

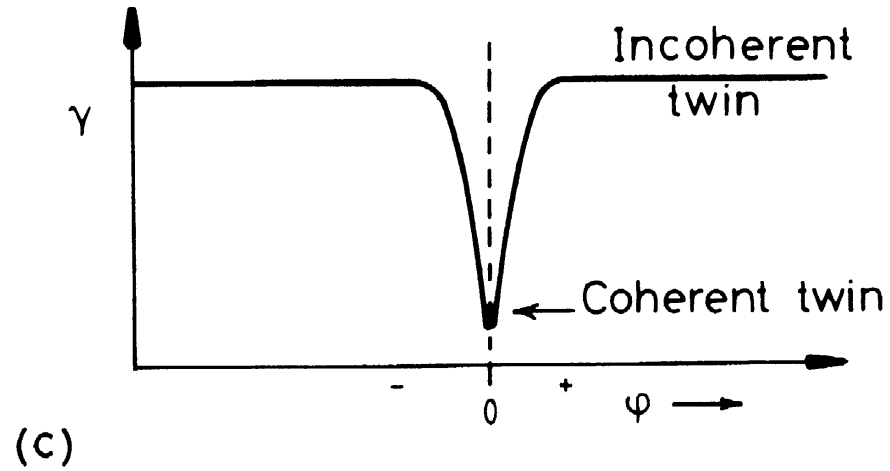

The torque term

Change in inclination causes a change in its energy, tending to twist it (either back or forwards)

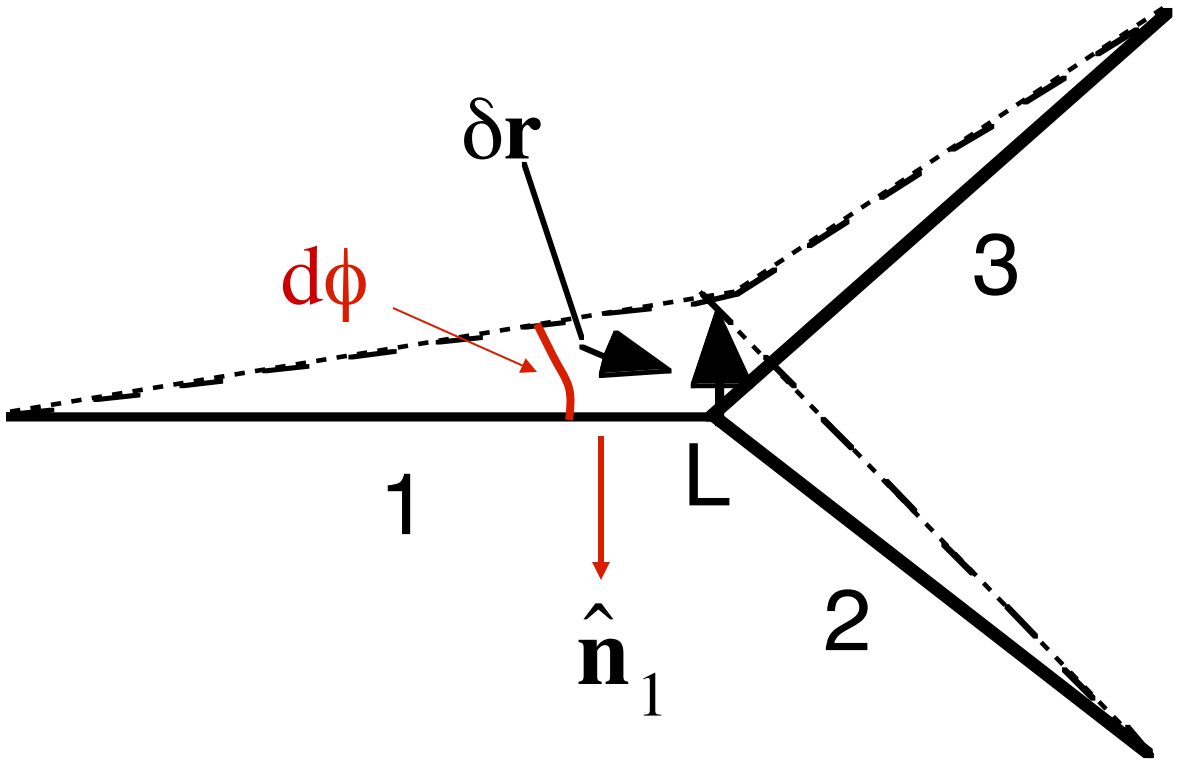

Inclination Dependence, contd.

- For local equilibrium at a TJ, what matters is the rate of change of energy with inclination, i.e. the *torque* on the boundary.
- Recall that the virtual displacement twists each boundary, i.e. changes its inclination.
- Re-express the force balance as ($\sigma \equiv \gamma$):

surface tension terms

$$\sum_{j=1}^{3} \left\{ \sigma_j \hat{b}_j + \left(\partial \sigma_j / \partial \phi_j \right) \hat{n}_j \right\} = \vec{0}$$

torque terms

Herring's Relations

$$\gamma_i \hat{t}_i + \hat{n}_i \frac{\partial \gamma_i}{\partial \theta} = 0$$

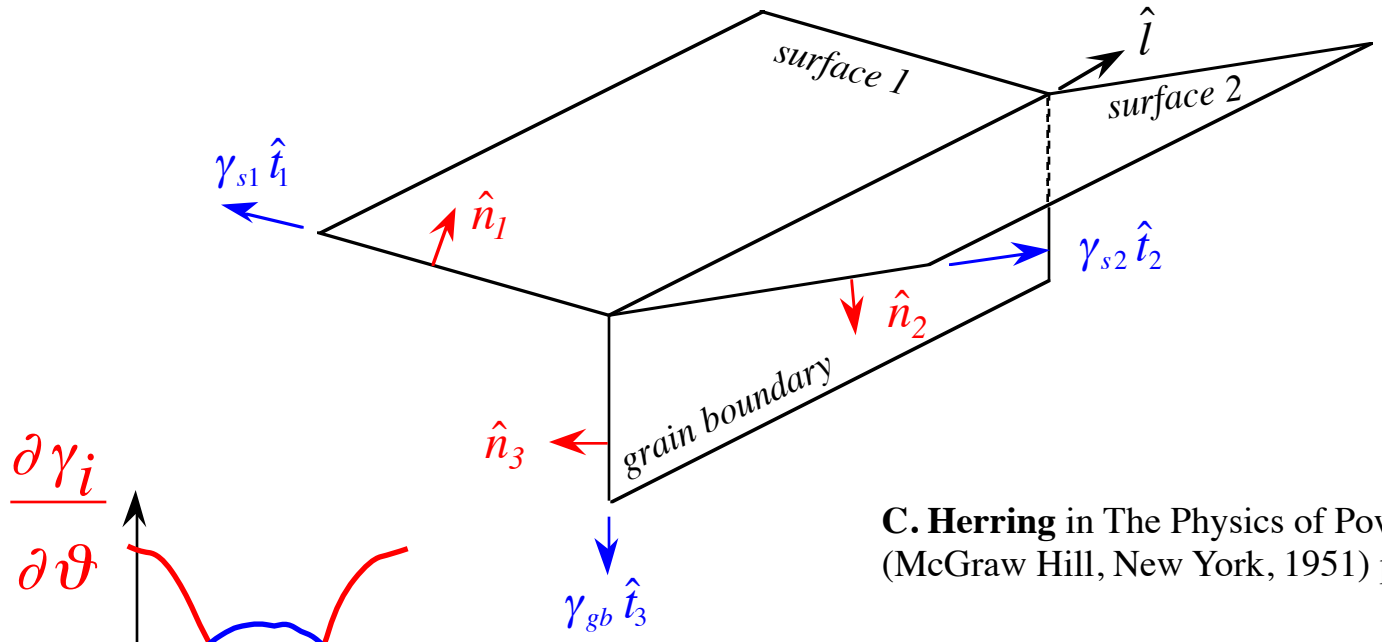

C. Herring in The Physics of Powder Metallurgy. (McGraw Hill, New York, 1951) pp. 143-79

NB: the torque terms can be just as large as the surface tensions

Torque effects

- The effect of inclination seems esoteric: should one be concerned about it?
- Yes! Twin boundaries are only one example where inclination has an obvious effect. Other types of grain boundary (to be explored later) also have low energies at unique misorientations.
- Torque effects can result in inequalities* instead of equalities for dihedral angles.

* B.L. Adams, et al. (1999). "Extracting Grain Boundary and Surface Energy from Measurement of Triple Junction Geometry." Interface Science **7**: 321-337.

Aluminum foil, cross section

- Torque term literally twists the boundary away from being perpendicular to the surface

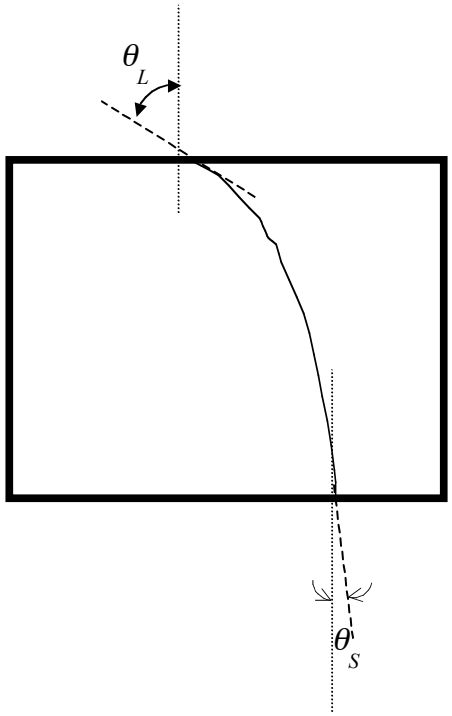

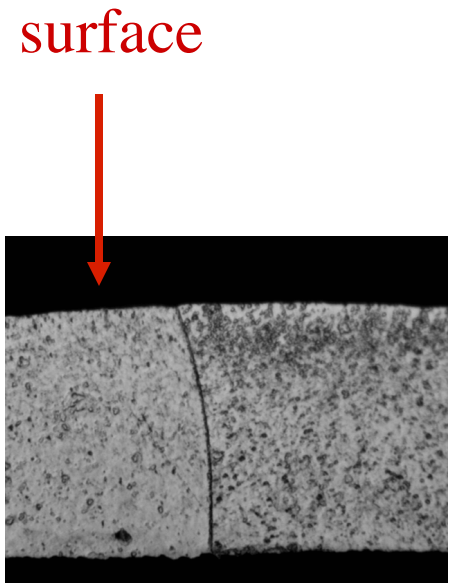

Why Triple Junctions?

- For isotropic g.b. energy, 4-fold junctions split into two 3-fold junctions with a reduction in free energy:

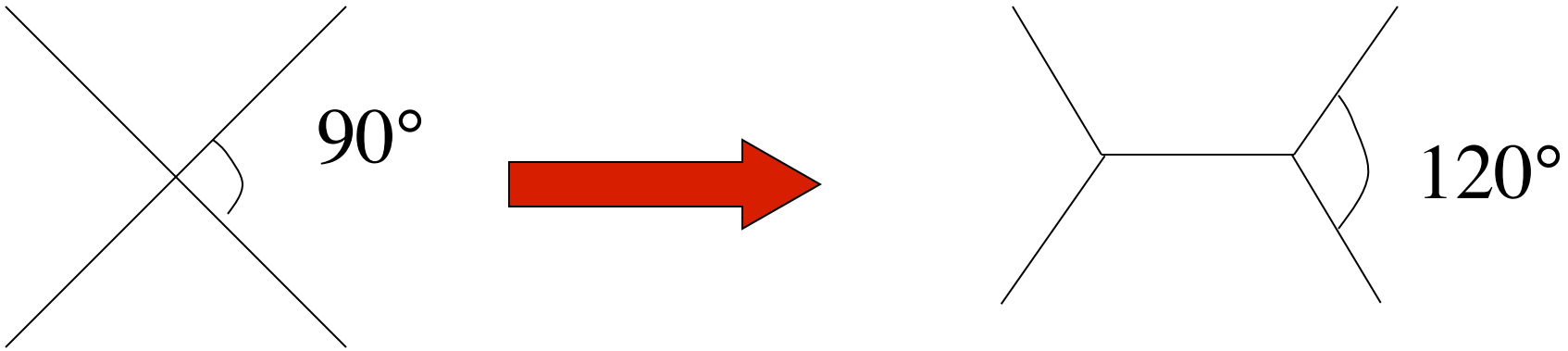

How to Measure Dihedral Angles and Curvatures: 2D microstructures

(1)

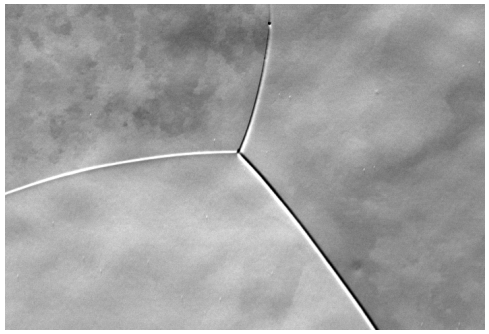

Image Processing

(2) Fit conic sections to each grain boundary:

$$Q(x,y)=Ax^2+ Bxy+ Cy^2+ Dx+ Ey+F = 0$$

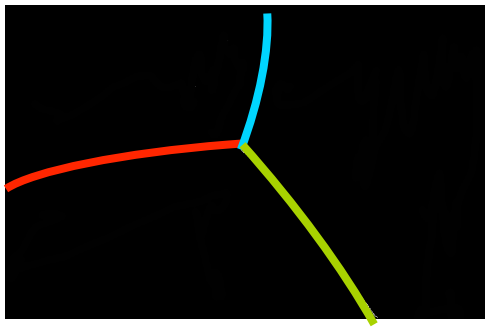

Assume a quadratic curve is adequate to describe the shape of a grain boundary.

"Measuring relative grain boundary energies and mobilities in an aluminum foil from triple junction geometry", C.-C. Yang, W. W. Mullins and A. D. Rollett, *Scripta Materialia* **44**: 2735-2740 (2001).

Measuring Dihedral Angles and Curvatures

(3) Calculate the tangent angle and curvature at a triple junction from the fitted conic function, Q(x,y):

$$y' = \frac{dy}{dx} = \frac{-(2Ax + By + D)}{Bx + 2Cy + E}$$

$$y'' = \frac{d^2y}{dx^2} = \frac{-(2A + 2By' + 2Cy'^2)}{2Cy + Bx + E}$$

$$\kappa = \frac{y''}{(1 + y'^2)^{\frac{3}{2}}}; \qquad \theta_{\tan} = \tan^{-1} y'$$

$Q(x,y)=Ax^2+ Bxy + Cy^2+ Dx+ Ey+F=0$

Application to G.B. Properties

- In principle, one can measure many different triple junctions to characterize crystallography, dihedral angles and curvature.
- From these measurements one can extract the relative properties of the grain boundaries.

Energy Extraction

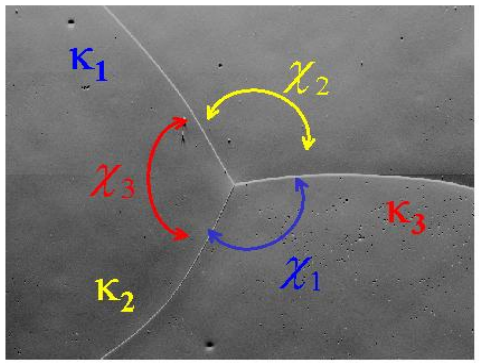

$$\begin{cases} (sin\chi_2)\ \sigma_1 - (sin\chi_1)\ \sigma_2 = 0 \\ (sin\chi_3)\ \sigma_2 - (sin\chi_2)\ \sigma_3 = 0 \end{cases}$$

$$\rightarrow \begin{pmatrix} sin\chi_2 & -sin\chi_1 & 0 & 0 & \ldots 0 \\ 0 & sin\chi_3 & -sin\chi_2 & 0 & \ldots 0 \\ * & * & 0 & 0 & \ldots 0 \\ : & : & : & : & : \\ 0 & 0 & * & * & 0 \end{pmatrix} \begin{pmatrix} \sigma_1 \\ \sigma_2 \\ \sigma_3 \\ : \\ \sigma_n \end{pmatrix} = 0$$

Measurements at many TJs; bin the dihedral angles by g.b. type; average the sinχ; each TJ gives a pair of equations

D. Kinderlehrer *et al.* , Proc. of the Twelfth International Conference on Textures of Materials (ICOTOM), Montréal, Canada, (1999) p1643.
K. Barmak *et al.*, "Grain boundary energy and grain growth in Al films: Comparison of experiments and simulations", *Scripta Mater.*, **54** (2006) 1059-1063: **following slides …**

Determination of Grain Boundary Energy via a Statistical Multiscale Analysis Method

- Assume:
  - Equilibrium at the triple junction (TJ)
  - Grain boundary energy to be independent of grain boundary inclination
- Sort boundaries according to misorientation angle (θ) – use 2° bins
- Symmetry constraint: $\theta \leq 62.8°$

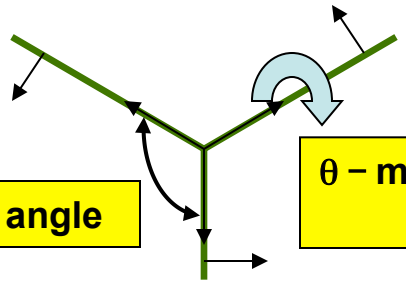

χ – **dihedral angle**

θ – **misorientation angle**

K. Barmak, et al.

Type	Misorientation Angle
1	1.1-4
2	4.1-6
3	6.1-8
4	8.1-10
5	10.1-15
6	15.1-18
7	18.1-26
8	26.1-34
9	34.1-42
10	42.1-46
11	46.1-50
12	50.1-54
13	54.1-60

Example: $\{001\}^c$ $[001]^s$ textured Al foil

Equilibrium at Triple Junctions

Herring's Eq.

$$\sum_{j=1}^{3}\left\{\sigma_j \hat{b}_j + \left[\frac{\partial \sigma_j}{\partial \phi_j}\right]\hat{n}_j\right\} = \vec{0}$$

Young's Eq.

$$\frac{\sigma_1}{\sin\chi_1} = \frac{\sigma_2}{\sin\chi_2} = \frac{\sigma_3}{\sin\chi_3}$$

b_j - boundary tangent
n_j - boundary normal
χ - dihedral angle
σ - grain boundary energy

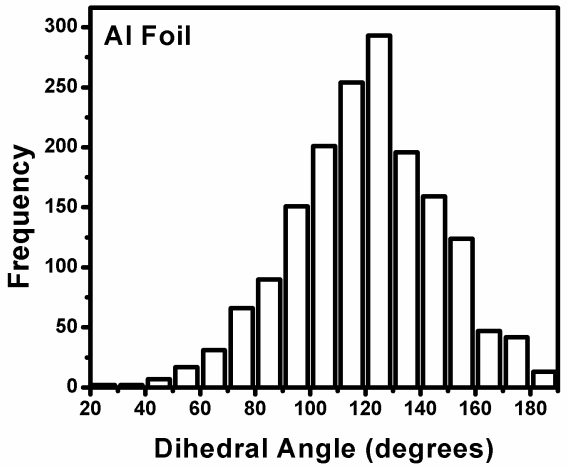

Example: $\{001\}^c$ $[001]^s$ textured Al foil

Since the crystals have strong {111} fiber texture, we **assume** ;
- all grain boundaries are pure {111} tilt boundaries
- the tilt angle is the same as the misorientation angle

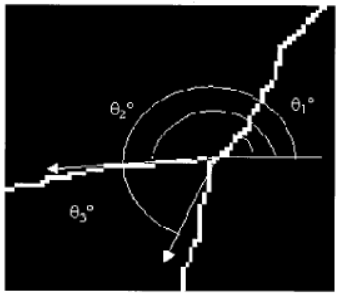

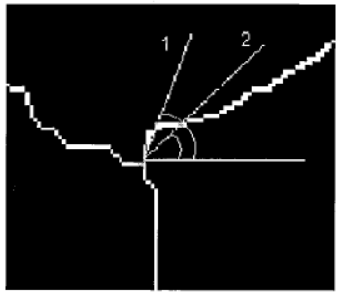

For example use Linefollow (Mahadevan et al.)

K. Barmak, et al.

Cross-Sections Using OIM

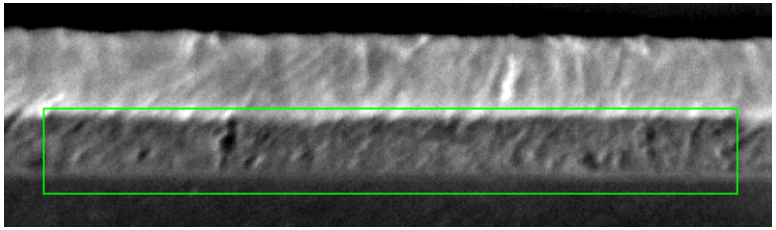

3 μm

SEM image

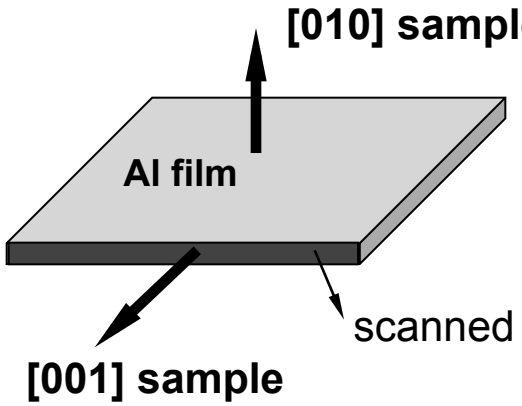

$[001]_{sample}$ inverse pole figure map, raw data

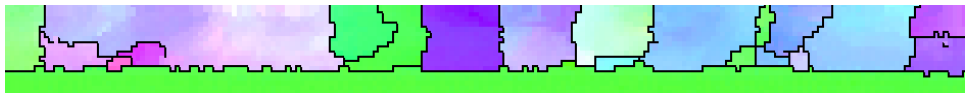

$[001]_{sample}$ inverse pole figure map, cropped cleaned data
- remove Cu (~0.1 mm)
- clean up using a grain dilation method (min. pixel 10)

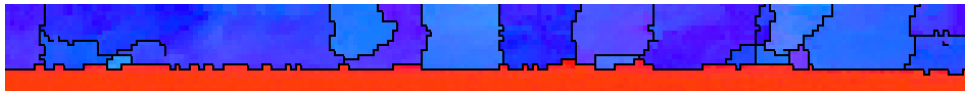

$[010]_{sample}$ inverse pole figure map, cropped cleaned data

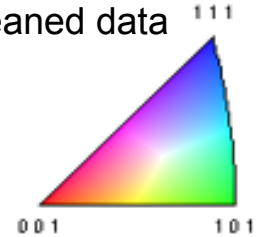

→ **Nearly columnar grain structure**

more examples

This film: $\{111\}_{crystal}$// $[010]_{sample}$ textured Al foil

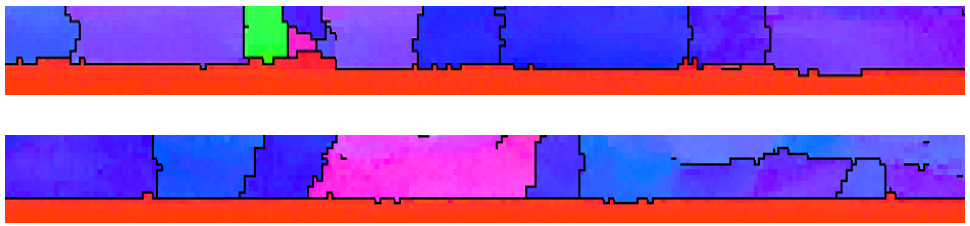

3 μm

K. Barmak, et al.

Grain Boundary Energy Calculation : Method

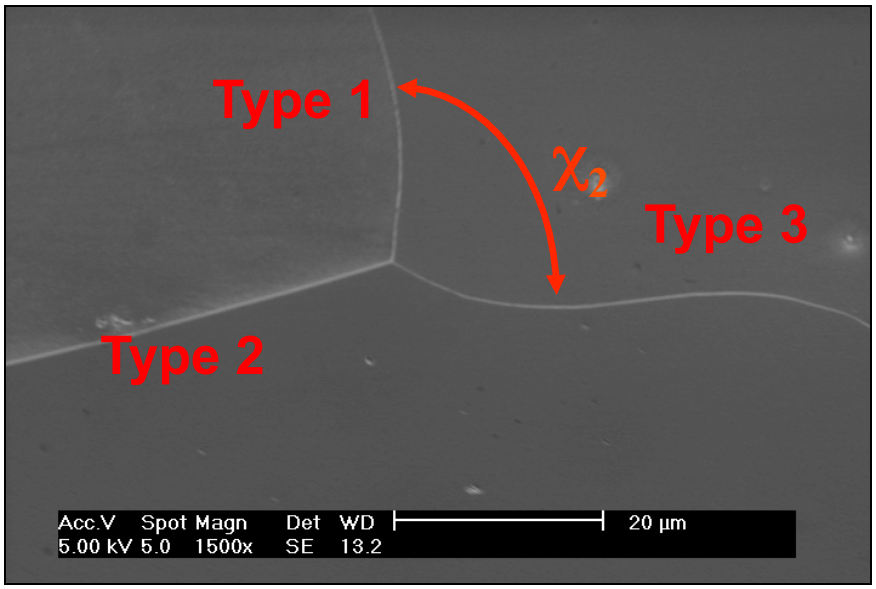

Type 1 - Type 2 = Type 2 - Type 1

Type 2 - Type 3 = Type 3 - Type 2

Type 1 - Type 3 = Type 3 - Type 1

Pair boundaries and put into urns of pairs

Young's Equation

$$\frac{\sigma_1}{\sin\chi_1} = \frac{\sigma_2}{\sin\chi_2} = \frac{\sigma_3}{\sin\chi_3}$$

⇨

Linear, homogeneous equations

$$\sigma_1 \sin\chi_2 - \sigma_2 \sin\chi_1 = 0$$
$$\sigma_2 \sin\chi_3 - \sigma_3 \sin\chi_2 = 0$$
$$\sigma_1 \sin\chi_3 - \sigma_3 \sin\chi_1 = 0$$

K. Barmak, et al.

Grain Boundary Energy Calculation : Method

N×(N-1)/2 equations
N unknowns

$$\sum_{j=1}^{N} A_{ij}\gamma_j = b_i \qquad \text{i=1,….,N(N-1)/2}$$

$$\begin{bmatrix}
\langle\sin\varphi_2\rangle & -\langle\sin\varphi_1\rangle & 0 & 0 & 0 & 0 & 0 & 0 & \cdots & 0 \\
\langle\sin\varphi_3\rangle & 0 & -\langle\sin\varphi_1\rangle & 0 & 0 & 0 & 0 & 0 & \cdots & 0 \\
\langle\sin\varphi_4\rangle & 0 & 0 & -\langle\sin\varphi_1\rangle & 0 & 0 & 0 & 0 & \cdots & 0 \\
\vdots & \vdots & \vdots & \vdots & \vdots & \vdots & \vdots & \vdots & \vdots & 0 \\
0 & \langle\sin\varphi_3\rangle & -\langle\sin\varphi_2\rangle & 0 & 0 & 0 & 0 & 0 & \cdots & 0 \\
0 & \langle\sin\varphi_4\rangle & 0 & -\langle\sin\varphi_2\rangle & 0 & 0 & 0 & 0 & \cdots & 0 \\
\vdots & \vdots & \vdots & \vdots & \vdots & \vdots & \vdots & \vdots & \vdots & \vdots \\
0 & 0 & 0 & 0 & 0 & 0 & 0 & 0 & \langle\sin\varphi_{N-1}\rangle & -\langle\sin\varphi_N\rangle
\end{bmatrix}
\begin{bmatrix}
\langle\gamma_1\rangle \\ \langle\gamma_2\rangle \\ \langle\gamma_3\rangle \\ \vdots \\ \langle\gamma_N\rangle
\end{bmatrix}
=
\begin{bmatrix}
0 \\ 0 \\ 0 \\ 0 \\ 0 \\ 0 \\ \vdots \\ 0
\end{bmatrix}$$

$$\underset{N}{\underset{N(N-1)/2}{\begin{pmatrix} \quad \end{pmatrix}}}\begin{pmatrix} \\ \\ \end{pmatrix}_{N} = \begin{pmatrix} \\ \\ \end{pmatrix}_{N(N-1)/2}$$

K. Barmak, et al.

Grain Boundary Energy Calculation : Summary

Assuming columnar grain structure and pure <111> tilt boundaries

# of total TJs : 8694
of {111} TJs : 7367 (10° resolution)
22101 (=7367×3) boundaries

calculation of dihedral angles
- reconstructed boundary line segments from TSL software

2° binning
(0°-1°, 1° -3°, 3° -5°, …,59° -61°,61° -62°)
32×31/2=496 pairs
no data at low angle boundaries (<7°)

$$\sum_{j=1}^{N} A_{ij}\gamma_j = b_i \qquad \text{i=1,….,N(N-1)/2}$$

Kaczmarz iteration method

B.L. Adams, D. Kinderlehrer, W.W. Mullins, A.D. Rollett, and Shlomo Ta'asan, Scripta Mater. 38, 531 (1998)

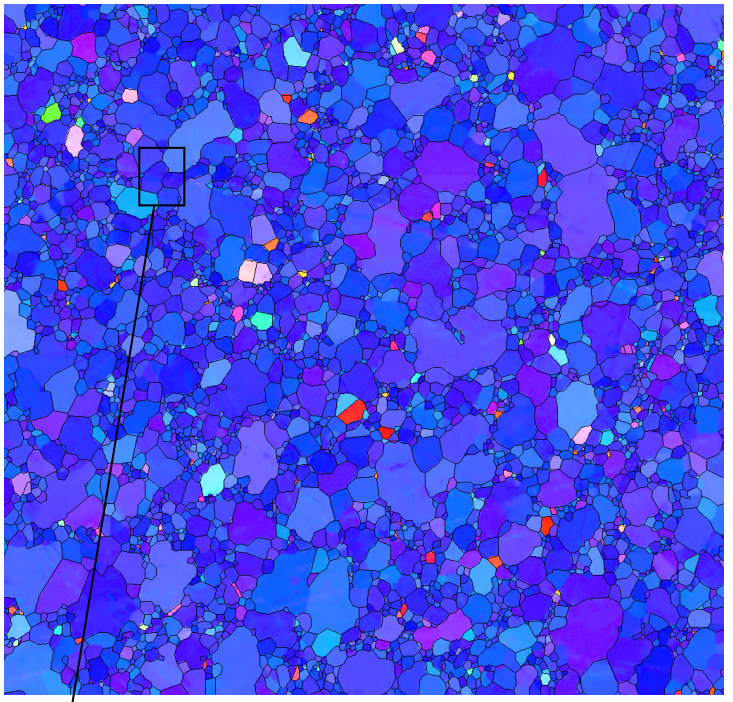

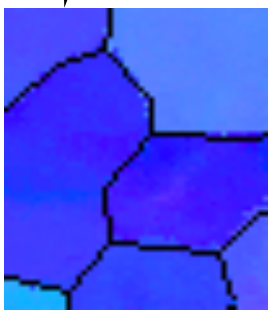

Reconstructed boundaries

This film: $\{111\}_{crystal}$// $[001]_{sample}$ textured Al foil

<111> Tilt Boundaries: Results

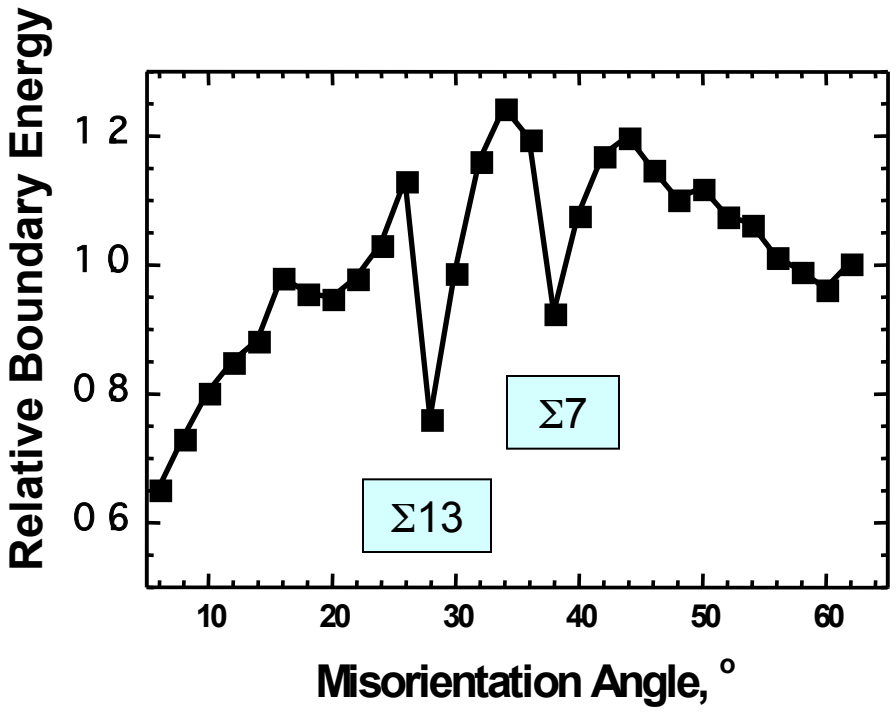

- Cusps at tilt angles of 28 and 38 degrees, corresponding to CSL type boundaries Σ13 and Σ7, respectively.

K. Barmak, et al.

Energy of High Angle Boundaries

- No universal theory exists to describe the energy of HAGBs.
- Based on a disordered atomic structure for general high angle boundaries, we expect that the g.b. energy should be at a maximum and approximately constant.
- Abundant experimental evidence for special boundaries at (a small number) of certain orientations for which the atomic fit is better than in general high angle g.b's.
- Each special point (in misorientation space) expected to have a cusp in energy, similar to zero-boundary case but with non-zero energy at the bottom of the cusp.
- Atomistic simulations suggest that g.b. energy is (positively) correlated with free volume at the interface. However, no simple way exists to predict the free volume based on the crystallographic type, so this does not help much.

Exptl. vs. Computed E_{gb}

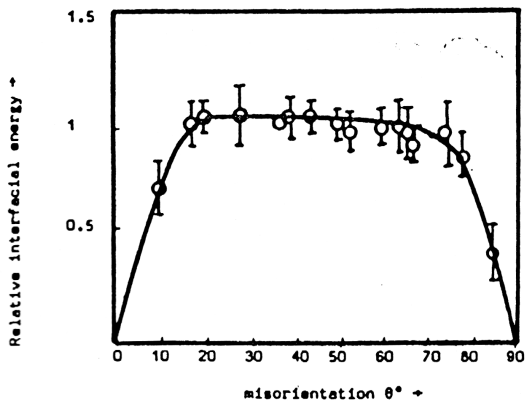

FIG. 1

Measured relative energies of [100] tilt boundaries in aluminium as a function of the misorientation θ (between [001] directions) The 37° [100] tilt boundary is used as reference for the energies.

<100> Tilts

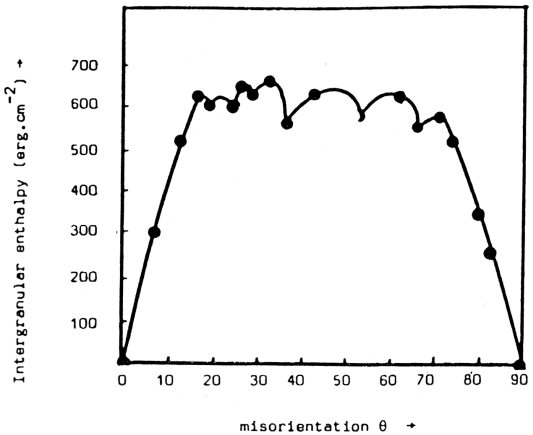

FIG. 3

Computed intergranular enthalpy of [100] tilt boundaries in aluminium as a function of misorientation θ (between [001] directions)

Σ11 with (311) plane

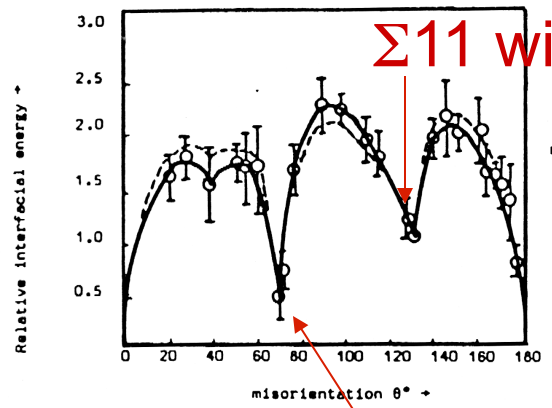

FIG. 2

Measured relative energies of [110] tilt boundaries in aluminium as a function of the misorientation θ (between [001] directions) The 129° 30' [110] tilt boundary is used as reference for the energies.

<110> Tilts

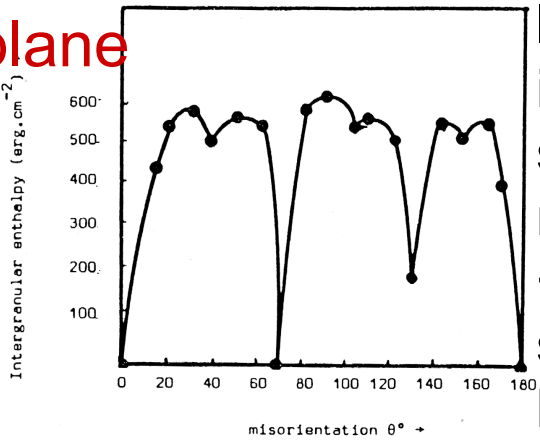

FIG. 4

Computed intergranular enthalpy of [110] tilt boundaries in aluminium as a function of misorientation θ (between [001] directions).

Note the presence of local minima in the <110> series, but not in the <100> series of tilt boundaries.

Σ3, 111 plane: CoherentTwin

Hasson & Goux, *Scripta metall.* **5** 889

Atomistic Calculations

- Olmsted, Foiles and Holm computed grain boundary energies for a set of 388 grain boundaries using molecular statics and embedded-atom interatomic potentials that represent nickel and aluminum ["Survey of computed grain boundary properties in face-centered cubic metals: I. Grain boundary energy,"*Acta Materialia* **57** (2009) 3694–3703].

Atomistic Calculations, contd.

- It is important to understand that each result i.e. an energy value for a particular grain boundary type, was the minimum value from a large number of trial configurations of that boundary.

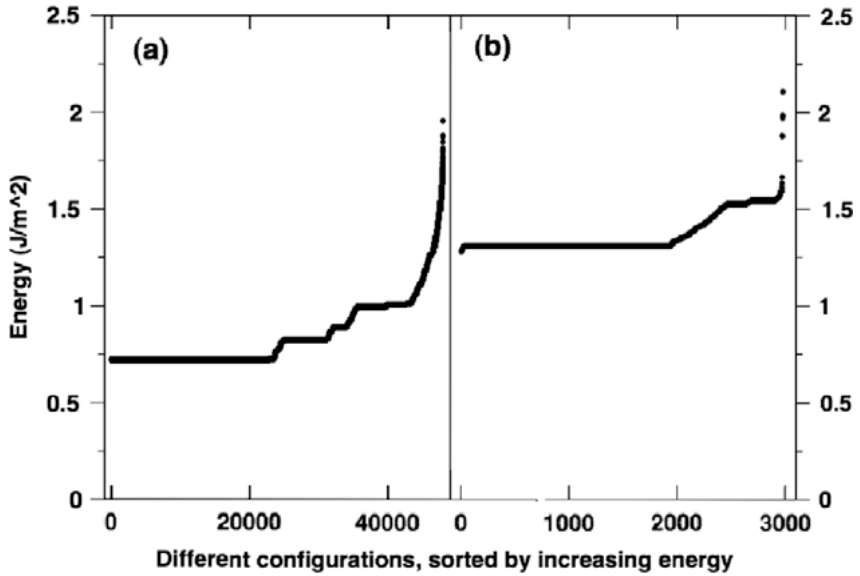

Fig. 1. The minimized energy of the set of initial structures discussed in the text for (a) a Σ111 grain boundary and (b) a asymmetric Σ5 (1 0 0)/(4 3 0) grain boundary. The energies are sorted by increasing energy in the plot. Note that in (a) about half of the initial structures yield the same, minimum, boundary energy, while in (b) a small number of boundaries have energies somewhat below the most common energy.

Olmsted *et al., Acta Materialia* **57** (2009) 3694

Atomistic Calculations, contd.

There are several key results. One is that, for any given CSL value, there is a wide range of energies, especially for 41 different Σ3 GBs. Also note that {111} twist boundaries are particularly low in energy, as expected from the argument about low energy surfaces giving low energy GBs. One outlier is the low energy Σ11 symmetric tilt with {113} normals. The excess free volume provides a weak correlation with energy, as previously noted.

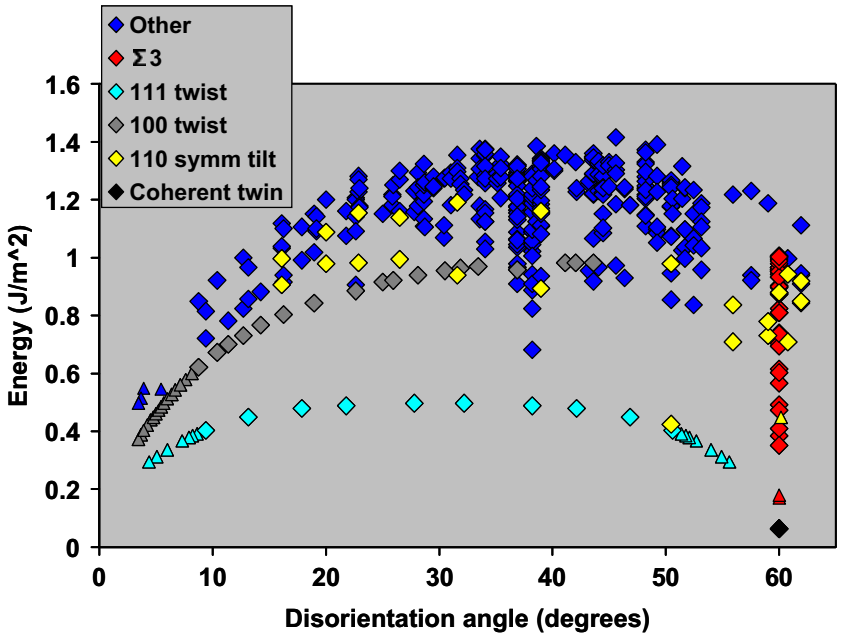

Fig. 2. The computed grain boundary energies for Ni plotted against the disorientation angle between the two grains. The red points correspond to Σ3 misorientations, the cyan points correspond to ⟨1 1 1⟩ twist grain boundaries, the grey symbols correspond to ⟨1 0 0⟩ twist grain boundaries, the yellow symbols correspond to ⟨1 1 0⟩ symmetric tilt grain boundaries and dark blue symbols correspond to all other boundaries. Triangles indicate data for boundaries outside the group of 388 boundaries defined by $L_{\max} = 15a_0/2$ as discussed in the text.

Acta Materialia **57** (2009) 3694

Atomistic Calculations, contd.

When the GB energies calculated in this manner for Al and Ni are compared, there is a very strong correlation. It appears that the proportionality factor is is very similar to the Voigt average shear modulus, which is the last entry in Table 1. This suggests (without proof!) that the properties of dislocations may be relevant to GB energy. This last point remains to be substantiated.

Acta Materialia **57** (2009) 3694

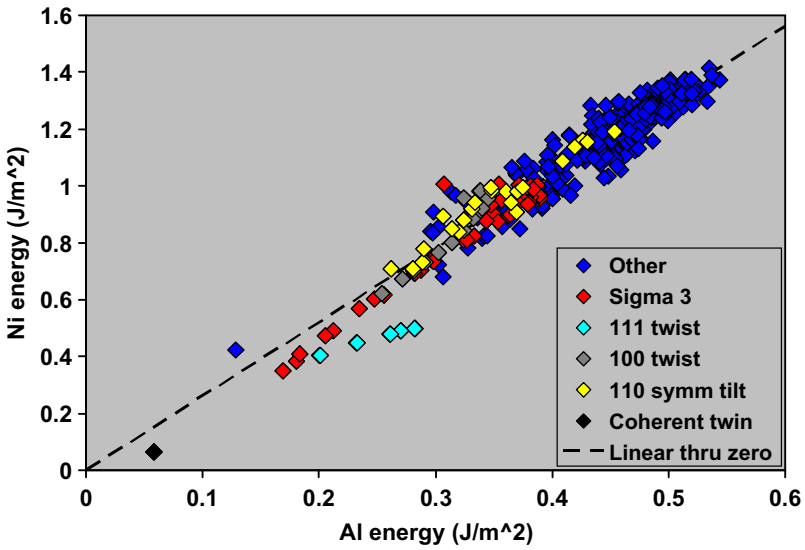

Fig. 7. Scatter plot of the computed grain boundary energies for Ni and Al. Each point represents the same macroscopic degrees of freedom though the microscopic structures may differ in some cases. The line indicates a by-hand linear fit constrained to pass through the origin to the data. The symbols are the same as in Fig. 2.

Table 1
The ratio of selected materials properties calculated for Ni and Al using the present interatomic potentials. The various properties are scaled by a power of the lattice constant, if needed, to obtain quantities with dimensions of energy/area. The properties listed are the melting temperature, sublimation energy, vacancy formation energy, stacking fault energy, free surface energies for (1 0 0), (1 1 0) and (1 1 1) faces, bulk modulus, the two extreme shear moduli and the Voigt average shear modulus.

Property	Ratio
$k_B T_M / a_0^2$	2.2
E_{sub} / a_0^2	1.7
E_v^f / a_0^2	3.3
γ_{sf}	1.2
$\gamma_{(1\,0\,0)}$	2.2
$\gamma_{(1\,1\,0)}$	2.3
$\gamma_{(1\,1\,1)}$	2.2
Ba_0	1.9
$C' a_0$	1.6
$C_{44} a_0$	2.8
$\mu_{voight} a_0$	2.4

Surface Energies vs. Grain Boundary Energy

- A recently revived, but still surprising to materials scientists, is that the grain boundary energy is largely determined by the energy of the two surfaces that make up the boundary (and that the twist angle is not significant).
- This is has been demonstrated to be highly accurate in the case of MgO, which is an ionic ceramic with a rock-salt structure. In this case, {100} has the lowest surface energy, so boundaries with a {100} plane are expected to be low energy.
- The next slide, taken from the PhD thesis work of David Saylor, shows a comparison of the GB energy computed as the average of the two surface energies, compared to the frequency of boundaries of the corresponding type. As predicted, the frequency is lowest for the highest energy boundaries, and vice versa.

2-Parameter Distributions: Boundary Normal only

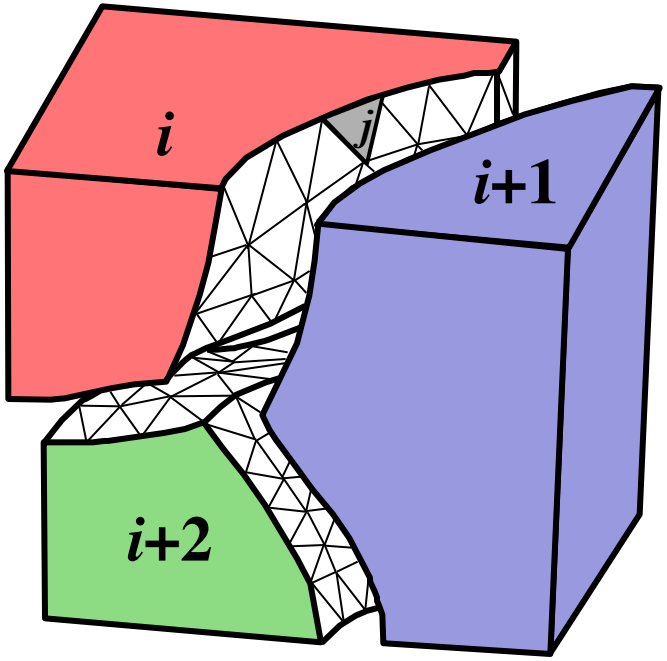

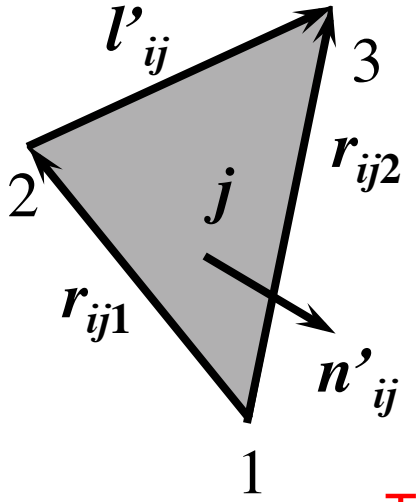

- **Index n' in the crystal reference frame:**
  $n = g_i n'$ and $n = g_{i+1} n'$
  (2 parameter description)

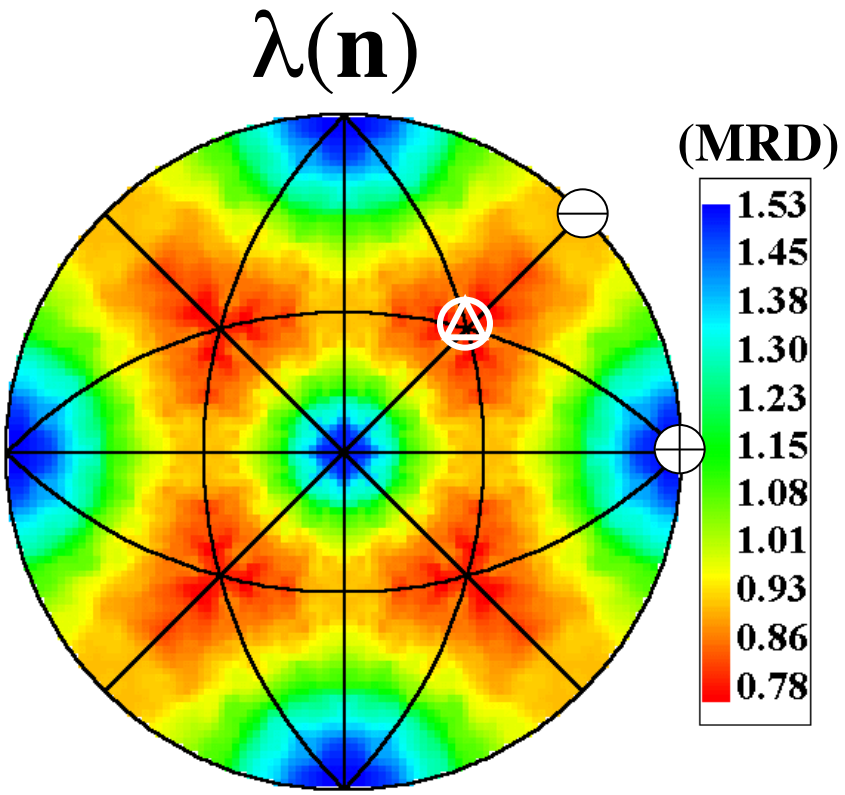

These are Grain Boundary Plane Distributions (GBPD)

Distribution of GB planes and energies in the crystal reference frame for Nickel

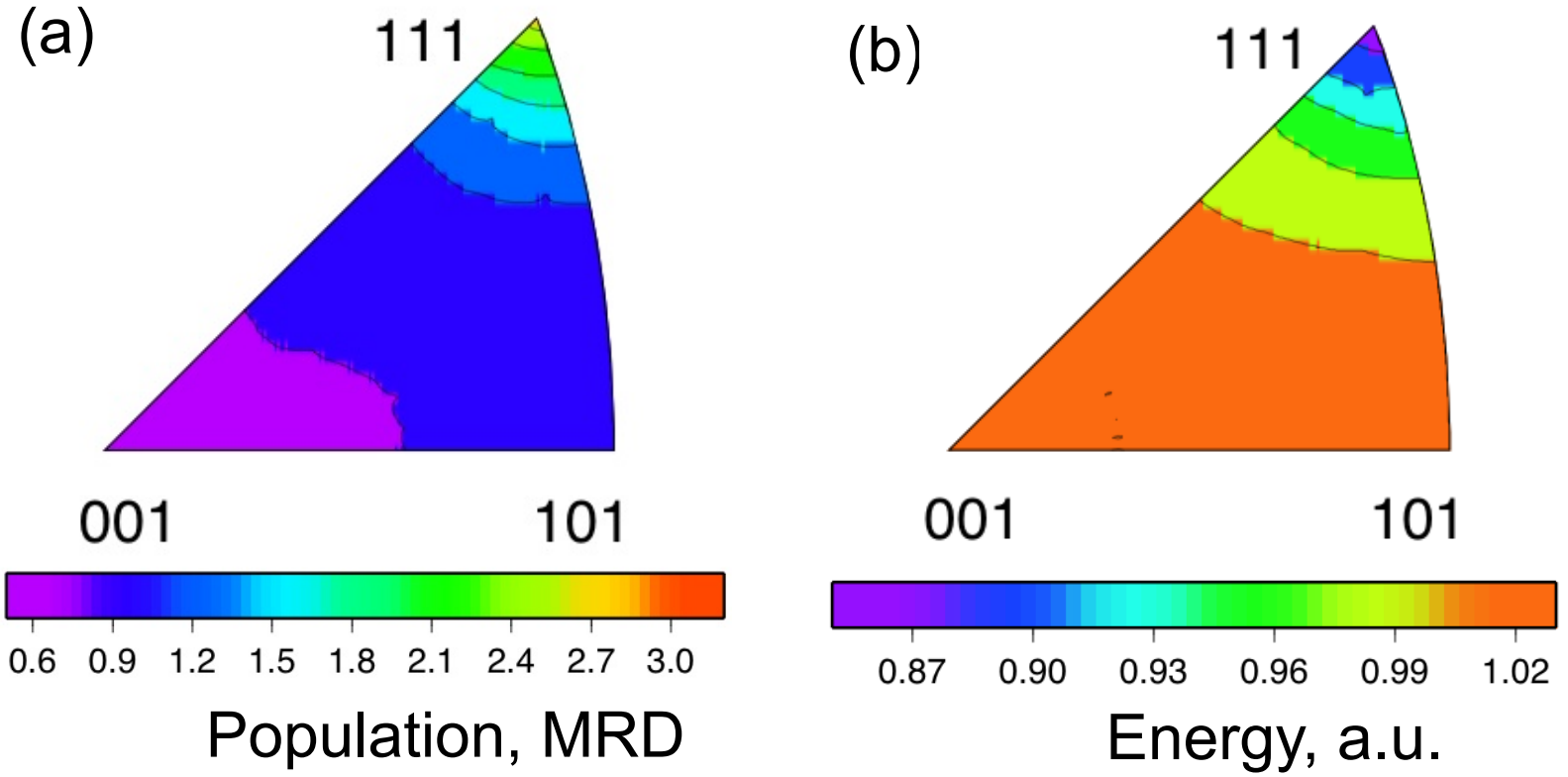

(111) planes have the highest population and the lowest relative energy (computed from dihedral angles)

Li et al., *Acta Mater.* **57** (2009) 4304

Distribution of GB planes and energies in the bicrystal reference frame

High purity Ni

Σ3 – Grain Boundary, Population and Energy

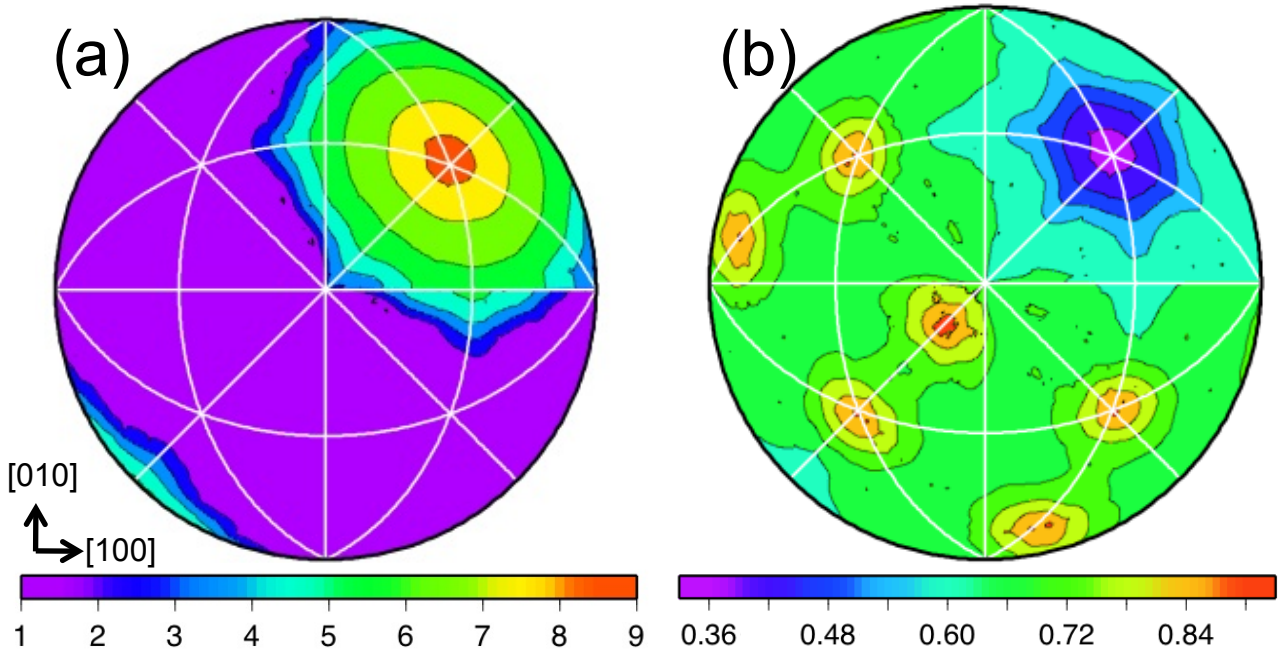

Boundary populations are inversely correlated with energy, although there are local variations

Li *et al.*, *Acta Mater.* **57** (2009) 4304

Sidebar
Simulations of grain growth with anisotropic grain boundaries shows that the GBCD develops as a consequence of energy but *not* mobility;
Gruber *et al.* (2005) *Scripta mater.* **53** 351

Theoretical versus Experimental GB Energies

Recent experimental [*Acta mater.* **57** (2010) 4304; *Acta mater.* **59** (2011) 5250] and computational studies [*Acta Mater.* **57** (2009) 3694] have produced two large grain boundary energy data sets for Ni. Using these results, we perform the first large-scale comparison between measured and computed grain boundary energies. While the overall correlation between experimental and computed energies is minimal, there is excellent agreement for the data in which we have the most confidence, particularly the experimentally prevalent Σ3 and Σ9 boundary types. Other CSL boundaries are infrequently observed in the experimental system and show little correlation with computed boundary energies. Because they do not depend on observation frequency, computed grain boundary energies are more reliable than the experimental energies for low population boundary types. Conversely, experiments can characterize high population boundaries that are not included in the computational study.

Unweighted fit

"Validating computed grain boundary energies in fcc metals using the grain boundary character distribution", Holm et al. *Acta mater.* (2011) **59** 5250

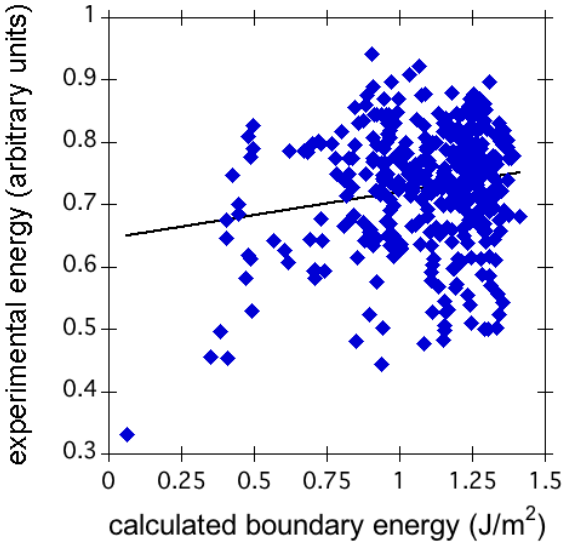

Weighted fit

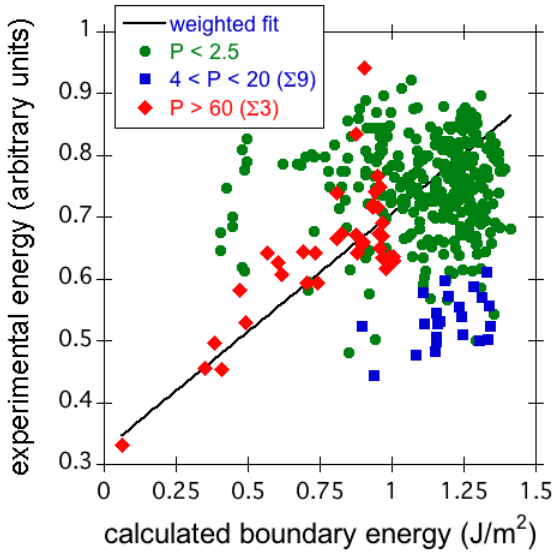

Theoretical versus Experimental GB Energies

[1] Li, *et al*. (2010) *Acta mater.* **57** 4304; [2] Rohrer, *et al*. (2010) *Acta mater.* **58** 5063

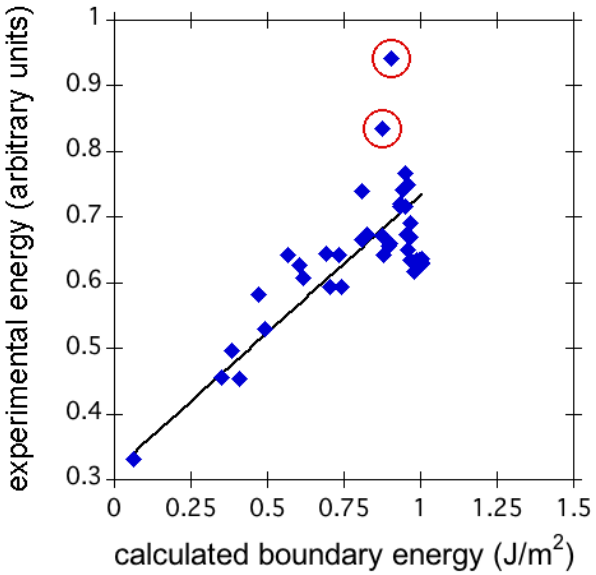

Regression for Σ9 boundaries ➔

Regression for Σ3 boundaries; outliers circled ➔

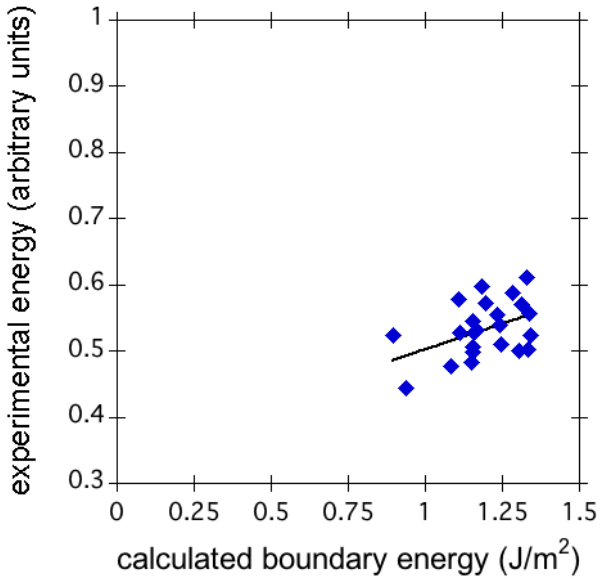

GB populations obtained from serial sectioning of fine grain (~5 μm) grain size pure Ni. GB energies calculated from dihedral angles at triple junctions. [1]

For high population Σ3 and mid population Σ9 boundaries, the inverse correlation between GBCD and GBED (solid lines) is stronger than the direct correlation between experimental and calculated GBEDs. However, the low population boundaries remain poorly correlated, due to high experimental uncertainty. [2]

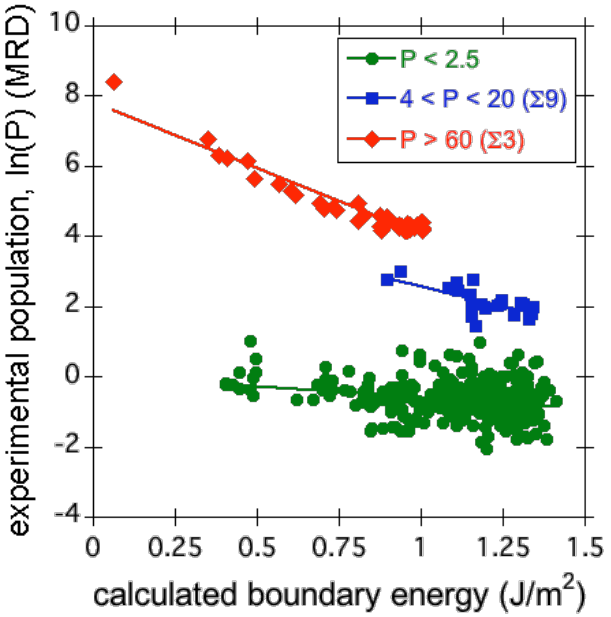

Grain Boundary Distribution in MgO: [100]

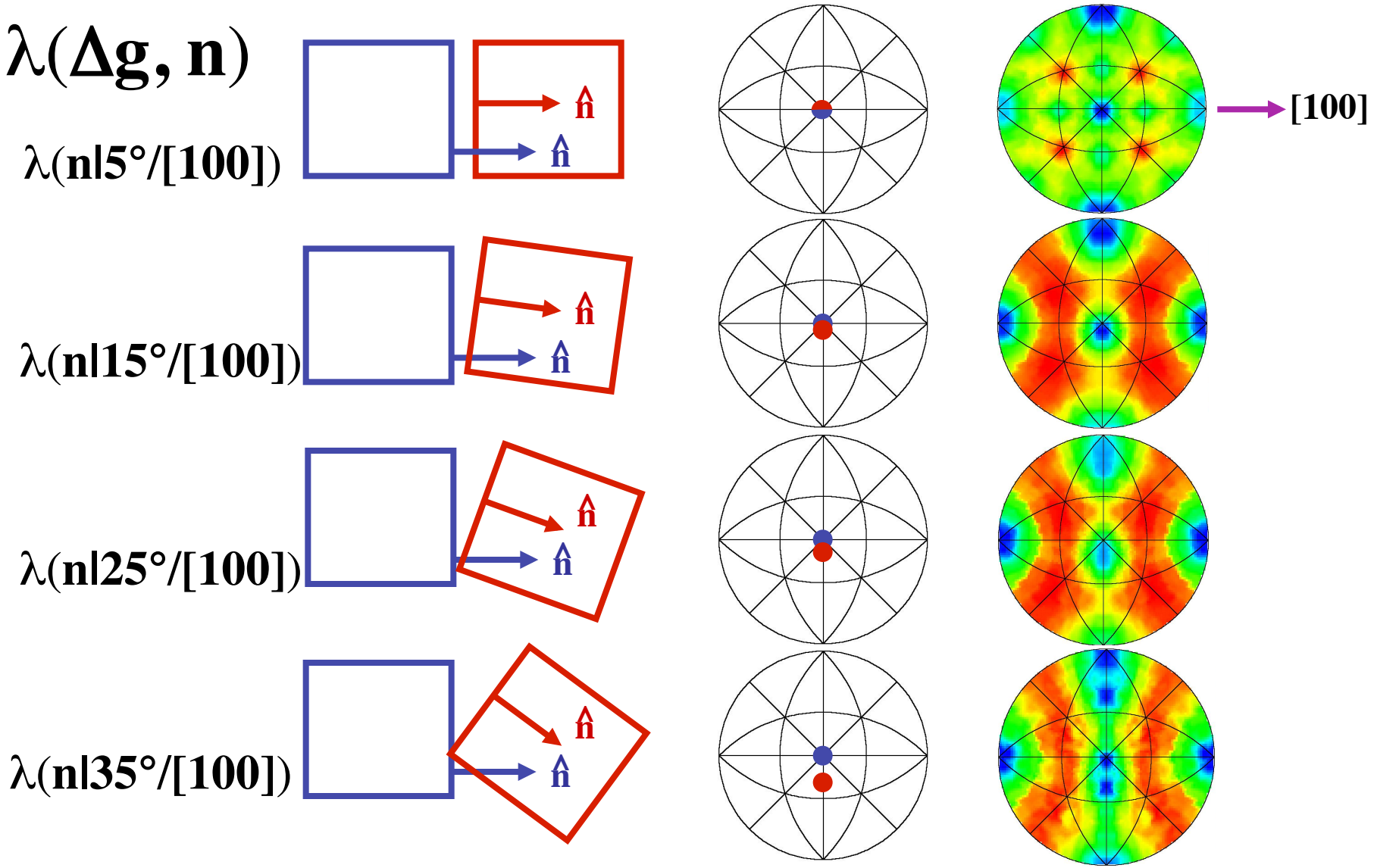

Every peak in λ(Δg,**n**) is related to a boundary with a {100} plane

Saylor DM, Morawiec A, Rohrer GS. Distribution and Energies of Grain Boundaries as a Function of Five Degrees of Freedom. *Journal of The American Ceramic Society* (2002) **85** 3081.

Examples of 2-Parameter Distributions

Grain Boundary Population (Δg averaged)

Measured Surface Energies

MgO

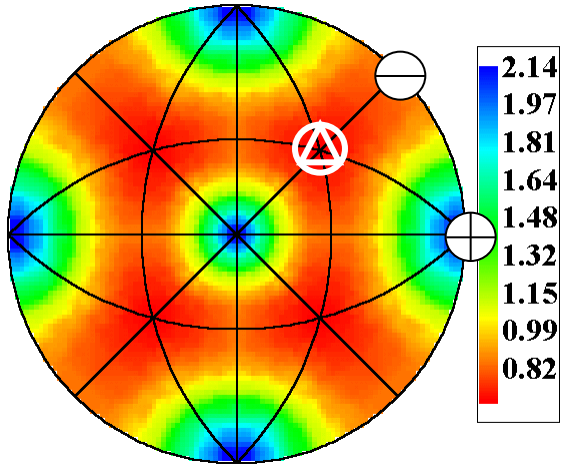

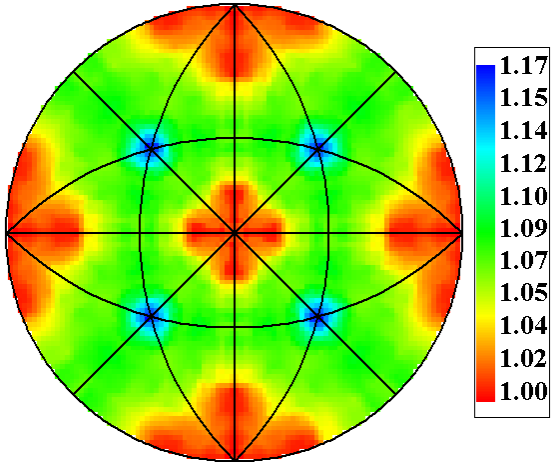

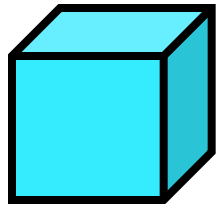

Saylor & Rohrer, Inter. Sci. 9 (2001) 35.

$SrTiO_3$

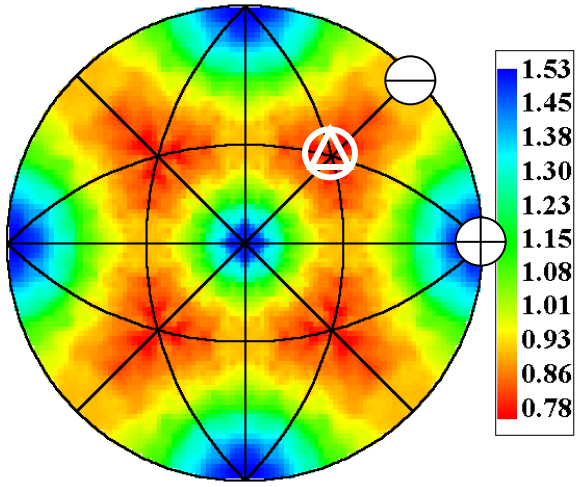

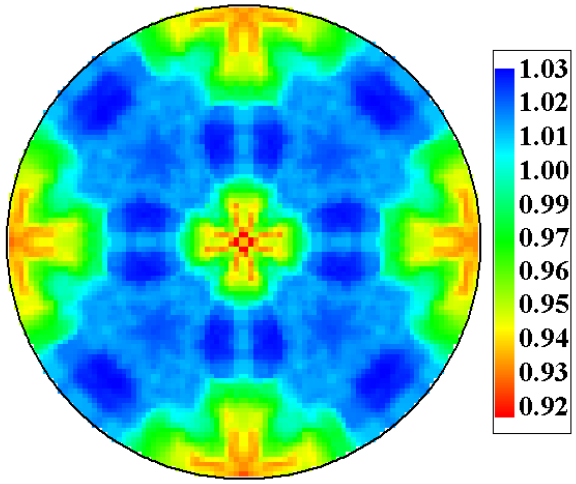

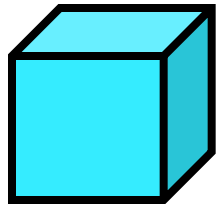

Sano et al., J. Amer. Ceram. Soc., 86 (2003) 1933.

Grain boundary energy and population

For all grain boundaries in MgO

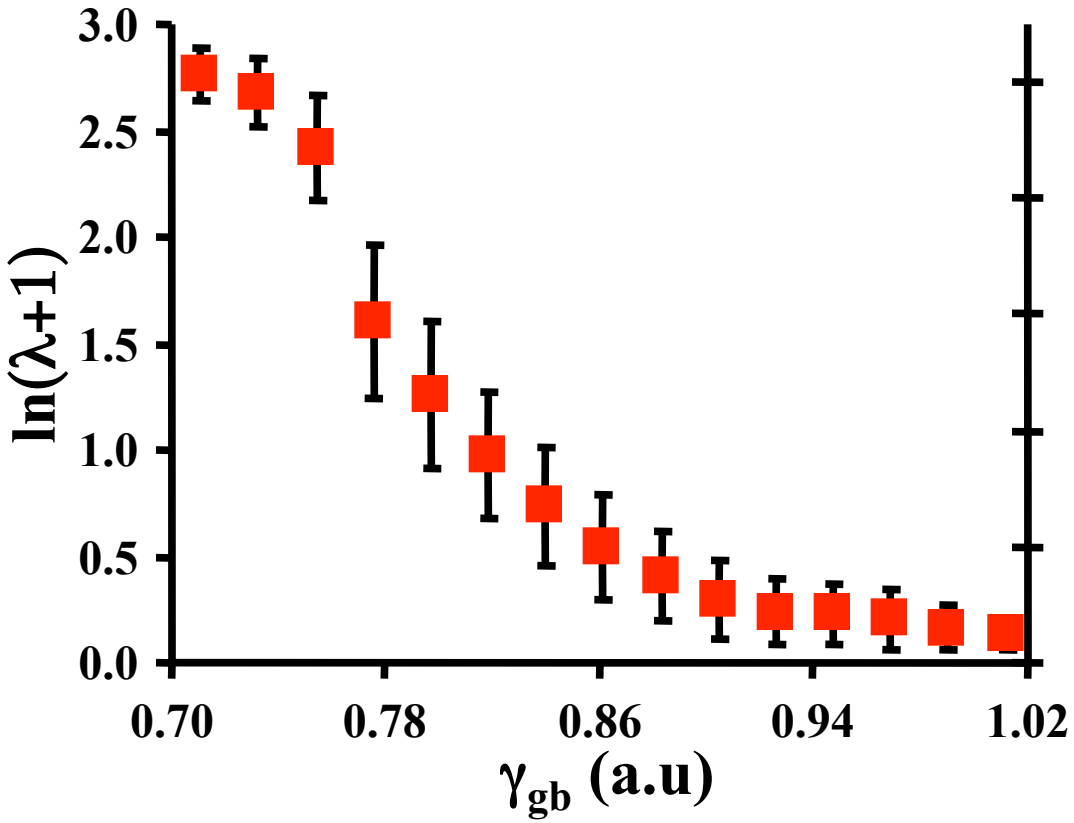

Population and Energy are *inversely correlated*

Saylor DM, Morawiec A, Rohrer GS. Distribution and Energies of Grain Boundaries as a Function of Five Degrees of Freedom. *Journal of The American Ceramic Society* (2002) **85** 3081.

Grain boundary energy and population

[100] misorientations in MgO

Grain boundary energy

$\gamma(\mathbf{n}|\omega/[\mathbf{100}])$

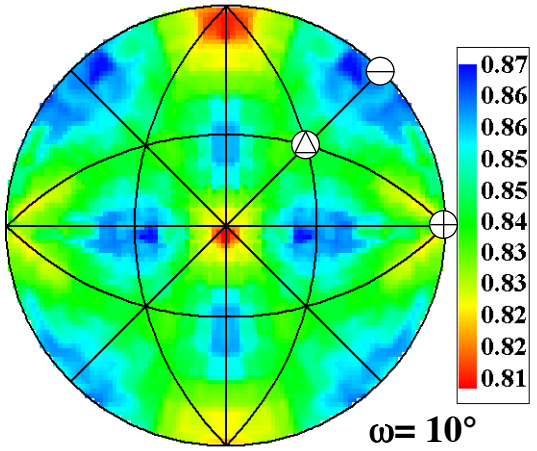

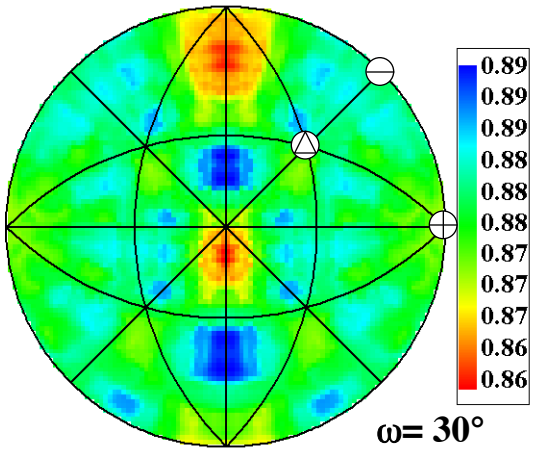

Grain boundary distribution

$\lambda(\mathbf{n}|\omega/[\mathbf{100}])$

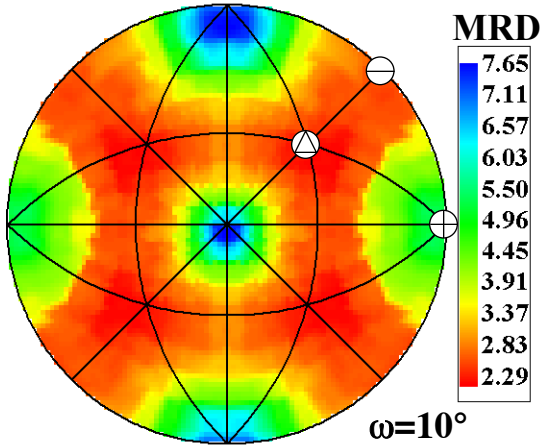

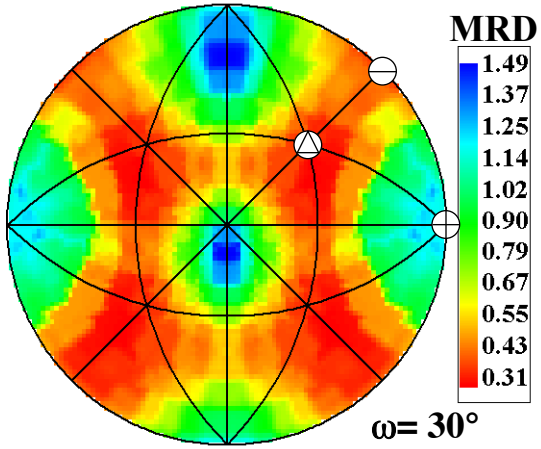

Population and Energy are inversely correlated

Saylor, Morawiec, Rohrer, Acta Mater. **51** (2003) 3675

Boundary energy and population in Al

Symmetric [110] tilt boundaries

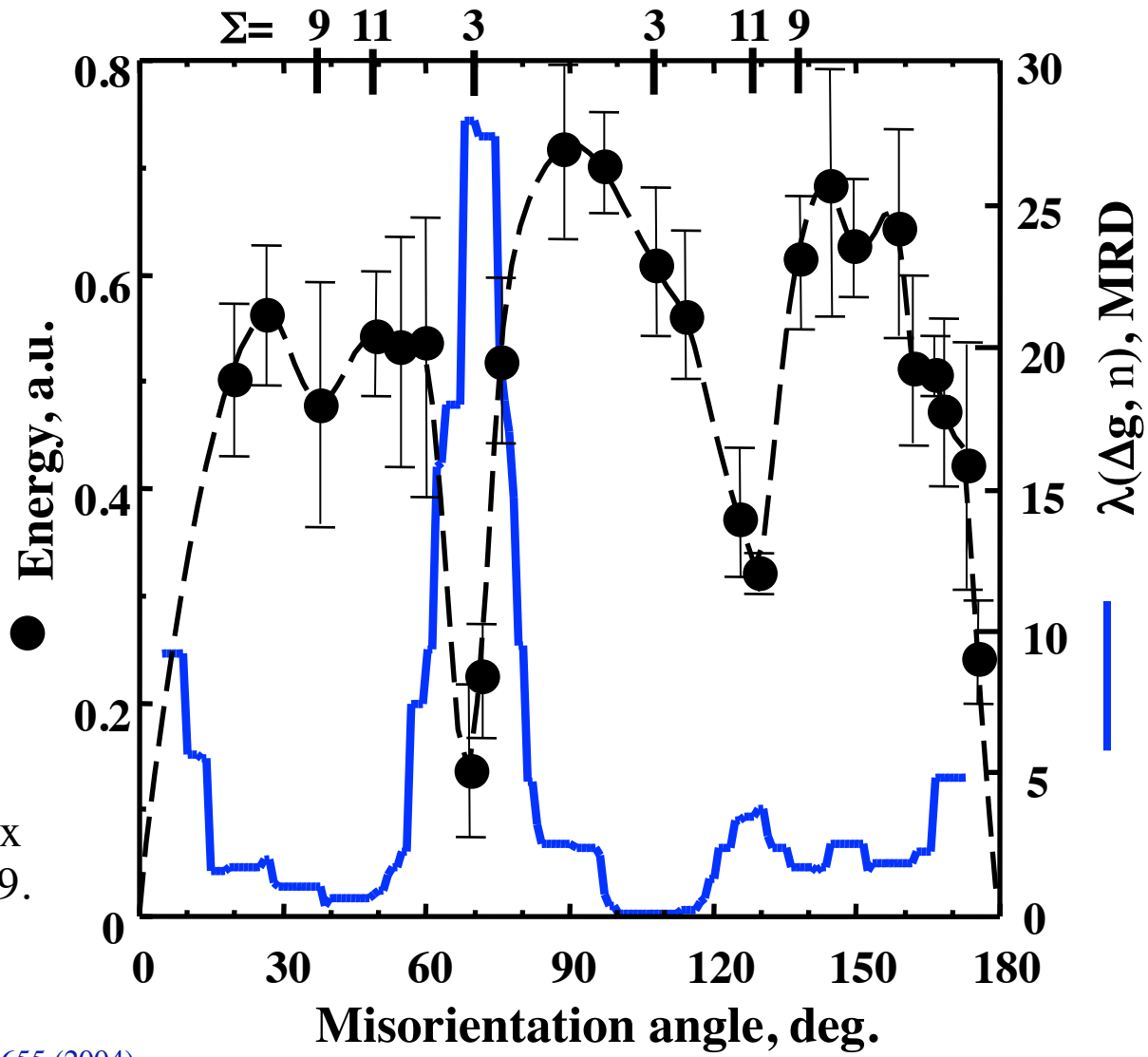

Energies:

G.C. Hasson and C. Goux
Scripta Met. 5 (1971) 889.

Al boundary populations:
Saylor et al. *Acta mater.*, **52**, 3649-3655 (2004).

Σ5 (37°/[100]) tilt boundaries in MgO

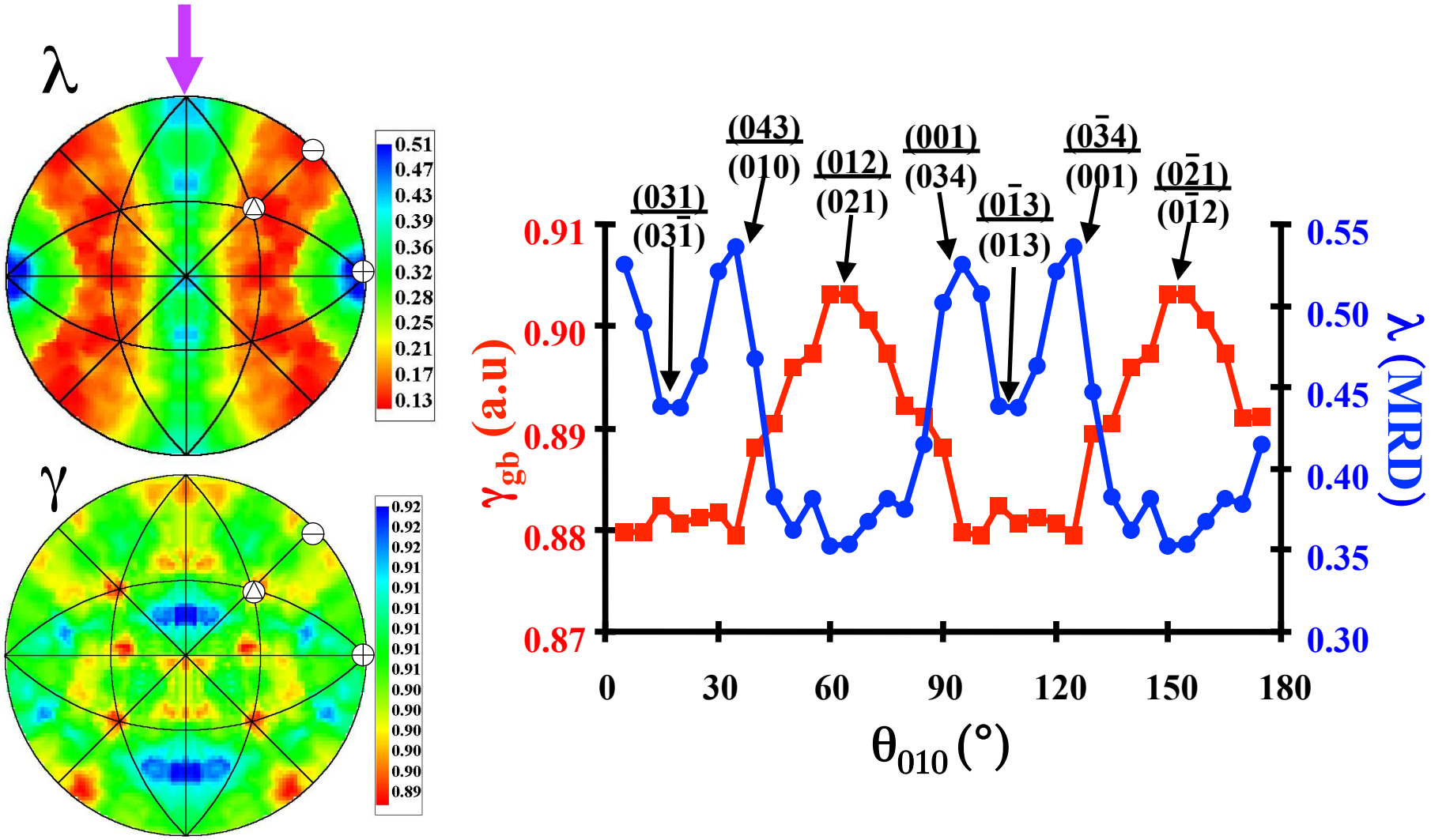

The energy-population correlation is not one-to-one

Computer Simulation of Grain Growth

- From the PhD thesis project of Jason Gruber.
- MgO-like grain boundary properties were incorporated into a finite element model of grain growth, i.e. minima in energy for any boundary with a {100} plane on either side.
- Simulated grain growth leads to the development of a g.b. population that mimics the experimental observations very closely.
- The result demonstrates that it is reasonable to expect that an anisotropic GB energy will lead to a stable population of GB types (GBCD).

Moving Finite Element Method

A.P. Kuprat: *SIAM J. Sci. Comput.* **22** (2000) 535. **G**radient **W**eighted **M**oving **F**inite **E**lements (LANL); PhD by Jason Gruber

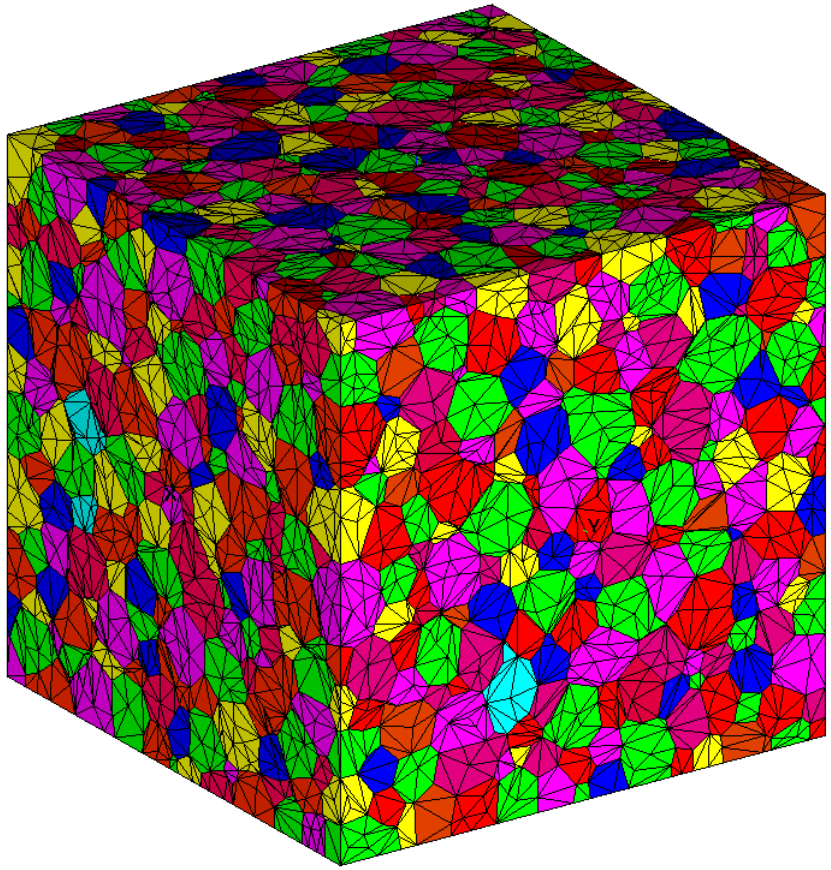

Elements move with a velocity that is proportional to the mean curvature

Initial mesh: 2,578 grains, random grain orientations (16 x 2,578 = 41,248)

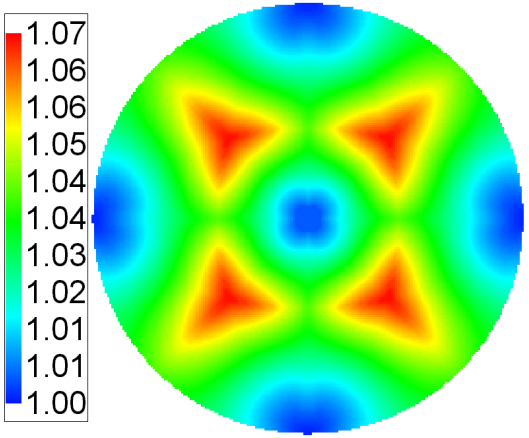

Energy anisotropy modeled after that observed for magnesia: minima on {100}.

GWMFE Results

- Input energy modeled after MgO
- Steady state population develops that correlates (inversely) with energy.

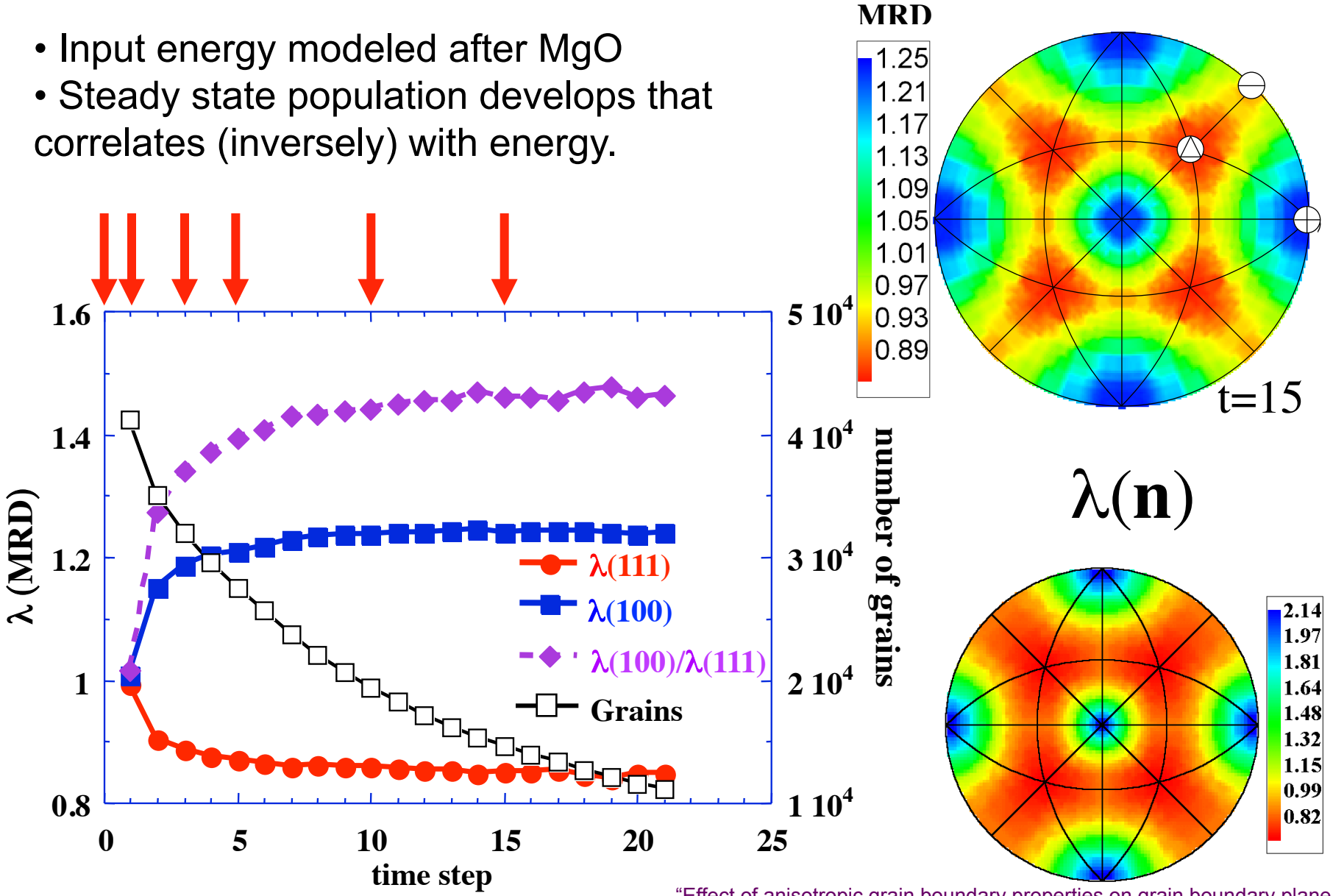

"Effect of anisotropic grain boundary properties on grain boundary plane distributions during grain growth", J. Gruber et al., *Scripta Mater.* **53** 351 (2005).

Population versus Energy

Experimental data: MgO

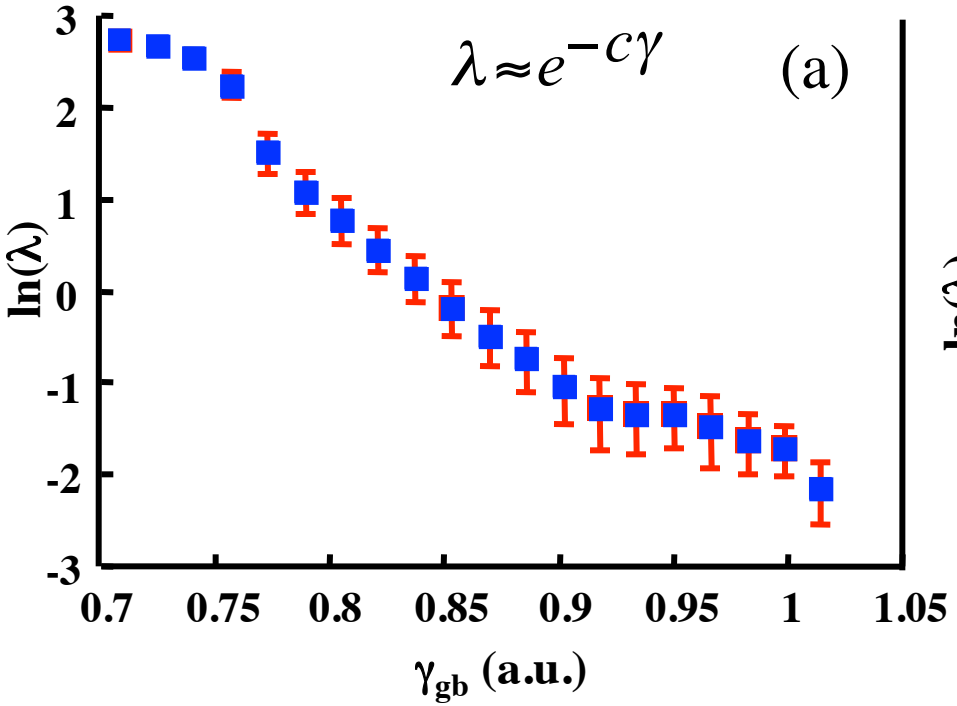

Simulated data:
Moving finite elements

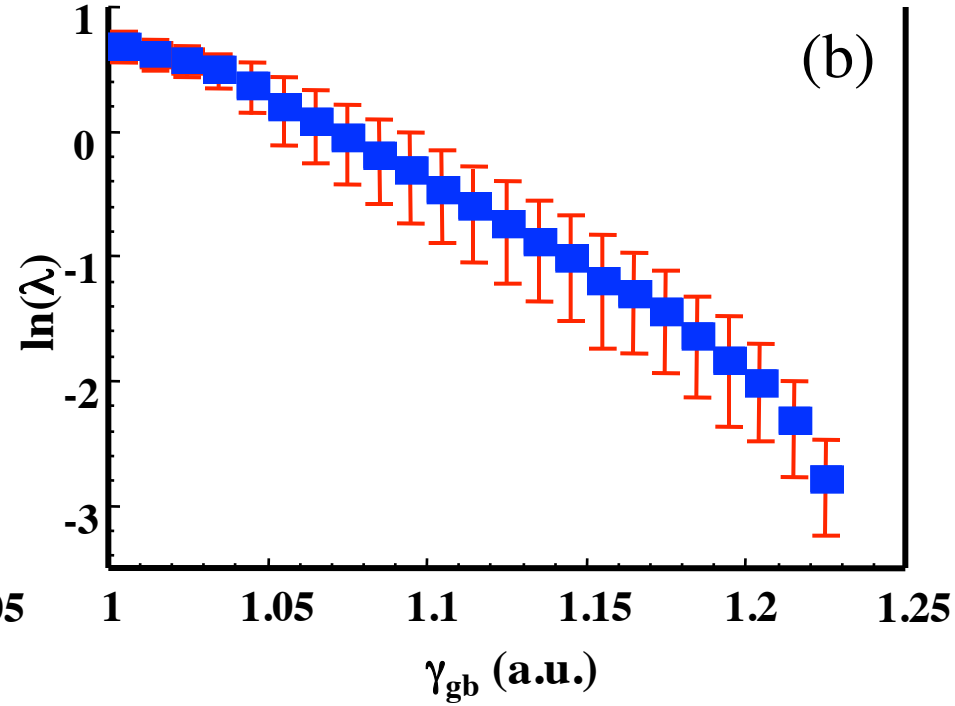

Energy and population are strongly correlated in both experimental results and simulated results. Is there a universal relationship?

Capillarity Vector, ξ

- The capillarity vector is a convenient quantity to use in force balances at junctions of surfaces.
- It is derived from the variation in (excess free) energy of a surface.
- In effect, the capillarity vector combines both the surface tension (so-called) and the torque terms into a single quantity

Hoffman, D. W. & Cahn, J. W., “A vector thermodynamics for anisotropic surfaces. I. Fundamentals and application to plane surface junctions.” *Surface Science* **31** 368-388 (1972).
Cahn, J. W. and D. W. Hoffman, "A vector thermodynamics for anisotropic surfaces. II. curved and faceted surfaces." *Acta metall*. **22** 1205-1214 (1974).

Equilibrium at TJ

- The utility of the capillarity (or "xi") vector, ξ, can be illustrated by re-writing Herring's equations as follows, where l_{123} is the triple line (tangent) vector.

$$(\xi_1 + \xi_2 + \xi_3) \times l_{123} = \mathbf{0}$$

- Note that the cross product with the TJ tangent implies resolution of forces perpendicular to the TJ.
- Used by the MIMP group to calculate the GB energy function for MgO. The numerical procedure is very similar to that outlined for dihedral angles, except now the vector sum of the capillarity vectors is minimized (Eq. above) at each point along the triple lines.

Morawiec A. "Method to calculate the grain boundary energy distribution over the space of macroscopic boundary parameters from the geometry of triple junctions", *Acta mater.* (2000) **48** 3525.
Also, Saylor D.M., Morawiec A., Rohrer G.S. "Distribution and Energies of Grain Boundaries as a Function of Five Degrees of Freedom" *J. American Ceramic Soc.* (2002) **85** 3081.

Capillarity vector definition

- Following Hoffman & Cahn, define a unit surface normal vector to the surface, $\hat{\mathbf{n}}$, and a scalar field, $r\gamma(\hat{\mathbf{n}})$, where r is a radius from the origin. Typically, the normal is defined with respect to crystal axes.

Capillarity vector: derivations

- Definition: $\xi = grad(r\gamma)$
- From which, Eq (1) $d(r\gamma) = grad(r\gamma) \cdot d\mathbf{r}$
- Giving, $d(r\gamma) = \xi \cdot (r d\hat{\mathbf{n}} + \hat{\mathbf{n}} dr)$
- Compare with the rule for products: $d(r\gamma) = r d\gamma + \gamma dr$

  gives: $\xi \cdot \hat{\mathbf{n}} = \gamma$ (2), and, $\xi \cdot d\hat{\mathbf{n}} = d\gamma$ (3)
- Combining total derivative of (2), with (3):

$$d\gamma - d\gamma = \xi\, d\hat{\mathbf{n}} + d\xi\, \hat{\mathbf{n}} - \xi \cdot d\hat{\mathbf{n}}$$

Eq (4): $0 = \hat{\mathbf{n}} \cdot d\xi$

Another useful result is the force, *f*, on an edge defined by a unit vector, *l*: $f = \xi \times \hat{l}$

Capillarity vector: components

- The physical consequence of Eq (2) is that the component of ξ that is normal to the associated surface, ξ_n, is equal to the surface energy, γ.

$$\xi_n = \gamma \hat{\mathbf{n}}$$

- Can also define a tangential component of the vector, ξ_t, that is parallel to the surface:

$$\xi_t = \xi - \gamma \hat{\mathbf{n}} = (\partial\gamma/\partial\theta)_{max} \hat{\mathbf{t}}_0$$

where the tangent vector is associated with the maximum rate of change of energy.

- With suitable manipulations, the Herring expression can be recovered.

G.B. Energy: Metals: Summary

- For low angle boundaries, use the Read-Shockley model with a *logarithmic dependence*: well established both experimentally and theoretically.
- For high angle boundaries, use a *constant value* unless (for fcc metals *only*) near a CSL structure related to the annealing twin (i.e. $\Sigma 3$, $\Sigma 9$, $\Sigma 27$, $\Sigma 81$ etc.) with high fraction of coincident sites *and* plane suitable for good atomic fit.
- In ionic solids, the grain boundary energy may be simply the average of the two surface energies (modified for low angle boundaries). This approach appears to be valid for metals also, although there are a few CSL types with special properties, e.g. highly mobile $\Sigma 7$ boundaries in fcc metals.

Summary

- Although the CSL theory is a useful introduction to what makes certain boundaries have special properties, grain boundary energy appears to be more closely related to the two surfaces comprising the boundary. This holds over a wide range of substances and means the g.b. energy is more closely related to surface energy than was previously understood. In *fcc* metals, however, certain CSL types are found in substantial fractions.

Questions: 1

- From the review of general properties:

1. What are the general features of the variation of GB mobility with GB type?
2. How does GB sliding vary with misorientation?
3. For <110> tilt boundaries in an fcc metal, how do you expect the GB diffusivity to vary with misorientation angle?

Questions: 2

- From the section on the Read-Shockley model

1. What is the functional form associated with Read-Shockley?
2. What is the physical basis for the R-S model?
3. If the misorientation axis is not, say <110>, is the single family of straight and parallel dislocations a reasonable picture of GB structure?
4. How do we typically partition between LAGB and HAGB?

Questions: 3

- From the section on energy measurement:

1. What does local equilibrium at a triple junction (line) mean?
2. How does help us measure variations in GB energy with crystallographic type?
3. What are Young's equations?
4. What are standard ways to measure GB energy?
5. Where does the "torque term" come from?
6. What are Herring's equations?
7. What is a way to parameterize a curve (in 2D)?
8. How do we use the information about dihedral angles to calculate GB energy?
9. What variation in GB energy was observed for <111> tilt GBs in Al?

Questions: 4

- From the section on High Angle GBs:
- What is a general rule for predicting HAGB energy?
- How do GB energies relate to surface energies?
- What is the evidence about <100> tilt GBs in MgO that tells us that surface energy dominates over, say, expecting a minimum GB energy for a symmetric tilt boundary?
- What does the evidence for <110> tilt boundaries in Al suggest?
- What correlation is generally observed for GB population and energy?
- Which GBs generally exhibit low energy in fcc metals?

Questions: 5

- Which GBs might be expected to exhibit low energy in bcc metals?
- What was the main result found by Gruber in his computer simulations?
- How is the capillarity vector constructed from a knowledge of the GB energy and the torque term?
- What is the practical value of the capillarity vector?

Supplemental Slides

Young Equns, with Torques

- Contrast the capillarity vector expression with the expanded Young eqns.:

$$\varepsilon_i = \frac{1}{\gamma_i}\frac{\partial \gamma_i}{\partial \phi_i}$$

$$\frac{\gamma_1}{\left(1-\varepsilon_2-\varepsilon_3\right)\sin\chi_1+\left(\varepsilon_3-\varepsilon_2\right)\cos\chi_1} =$$

$$\frac{\gamma_2}{\left(1-\varepsilon_1-\varepsilon_3\right)\sin\chi_2+\left(\varepsilon_1-\varepsilon_3\right)\cos\chi_2} =$$

$$\frac{\gamma_3}{\left(1-\varepsilon_1-\varepsilon_2\right)\sin\chi_3+\left(\varepsilon_2-\varepsilon_1\right)\cos\chi_3}$$

Expanded Young Equations

- Project the force balance along each grain boundary normal in turn, so as to eliminate one tangent term at a time:

$$\sum_{j=1}^{3}\left\{\sigma_j \hat{b}_j + \left(\frac{\partial\sigma}{\partial\phi}\right)_j \hat{n}_j\right\}\cdot n_1 = 0, \quad \varepsilon_i = \frac{1}{\sigma_i}\left(\frac{\partial\sigma}{\partial\phi}\right)_i$$

$$\sigma_1\varepsilon_1 + \sigma_2 \sin\chi_3 + \sigma_2\varepsilon_2 \cos\chi_3 - \sigma_3 \sin\chi_2 + \sigma_3\varepsilon_3 \cos\chi_2$$

$$\sigma_1\varepsilon_1\sigma_2 \sin\chi_3 / \sigma_2 \sin\chi_3 + \sigma_2 \sin\chi_3 + \sigma_2\varepsilon_2 \cos\chi_3 = \sigma_3 \sin\chi_2 + \sigma_3\varepsilon_3 \cos\chi_2$$

$$\left(1 + \sigma_1\varepsilon_1 / \sigma_2 \sin\chi_3\right)\sigma_2 \sin\chi_3 + \sigma_2\varepsilon_2 \cos\chi_3 = \sigma_3\left(\sin\chi_2 + \varepsilon_3 \cos\chi_2\right)$$

$$\left\{\left(1 + \sigma_1\varepsilon_1 / \sigma_2 \sin\chi_3\right)\sin\chi_3 + \varepsilon_2 \cos\chi_3\right\}\sigma_2 = \sigma_3\left(\sin\chi_2 + \varepsilon_3 \cos\chi_2\right)$$